TAMPEREEN TEKNILLINEN YLIOPISTO
TAMPERE UNIVERSITY OF TECHNOLOGY
Julkaisu 665 • Publication 665

Jani Lehto

Development and Characterization of Test Reactor with Results of Its Application to Pyrolysis Kinetics of Peat and Biomass Fuels

Tampere 2007

Tampereen teknillinen yliopisto. Julkaisu 665
Tampere University of Technology. Publication 665

Jani Lehto

Development and Characterization of Test Reactor with Results of Its Application to Pyrolysis Kinetics of Peat and Biomass Fuels

Thesis for the degree of Doctor of Technology to be presented with due permission for public examination and criticism in Konetalo Building, Auditorium K1702, at Tampere University of Technology, on the 7th of June 2007, at 12 noon.

Tampereen teknillinen yliopisto - Tampere University of Technology
Tampere 2007

ISBN 978-952-15-1775-4 (printed)
ISBN 978-952-15-1792-1 (PDF)
ISSN 1459-2045

To the memory of Aila Jokinen.

Abstract

The Finnish Government has strongly supported research on the exploitation of various biomass fuels at the expense of fossil fuels, which are one of the main contributors to the greenhouse effect. Biomass fuels are a widely available, renewable and CO_2-neutral energy source and are increasingly used as an alternative to fossil fuels for heat and energy supply. Peat is not completely CO_2-neutral. However, the annual growth of peatlands binds some of the CO_2 released during combustion. Hence, the classification of peat is somewhat unclear. The Finnish Government has proposed that peat could be classified as a slowly renewable natural resource. Moreover, peat and biomass fuels are important for the Finnish economy since they are indigenous fuels. Thus, exploitation is desirable not only due to their environmental but also due to their socio-economic effects.

Fluidized bed combustion has a long tradition in Finland. Especially the big pulp and paper industry in Finland has adopted flexible and reliable fluidized bed combustion for its steam and energy production system. Additionally, Finland has strong know-how in fluidized bed combustion since the world's leading fluidized bed boiler manufacturers have their offices in Finland.

It is known that several factors, such as temperature level and heating rate, have a strong effect on the volatile yield of a fuel during devolatilization. Even then the volatile content of a fuel is usually determined using slow-heating-rate standardized tests developed for coal or by thermogravimetry. Although these methods yield information on the volatile content of low-volatile-content fuels like coal, they do not work reliably with high-volatile-content fuels. As a result, neither the test methods developed for coal nor the results obtained from research on pyrolysis and combustion of coal can be directly adopted to peat and biomass cases. Instead, methods used in conditions more similar to those encountered in practical applications should be used for more accurate fuel characterization.

This dissertation concerns the pyrolysis of high-volatile-content fuels, such as biomass and peat. The dissertation also presents the development and characterization of a laboratory-scale test reactor for reliable determination of the volatile content of high-volatile-content fuels in conditions similar to those in fluidized bed boilers. Both experimental and modeling tools are used to study the pyrolysis characteristics of Finnish milled peat.

The volatile yield of Finnish milled peat at different residence times was determined using the developed reactor. Based on the experimental results, the kinetic parameters for Finnish milled peat are presented using two different kinetic models. Also, a method for estimating final volatile yield of peat pyrolysis is presented.

Preface

This work started while I was working at Metso Power in late 2003. For three years, through the year 2006, I worked at the Institute of Energy and Process Engineering at Tampere University of Technology to advance the academic aspects of the work. The work was finalised in the early 2007 while I was working again at Metso Power. This work was funded by Tekes (project 40121/04), Tampere University of Technology, Metso Power Oy, Foster Wheeler Energia Oy, VTT Technical Research Centre of Finland and Outokumpu Research Oy. I would like to thank all the financers and especially Tekes for organising the FB-Kupla project.

First of all, I would like to express my gratitude to my advisor, Professor Risto Raiko, for his guidance and support while preparing this dissertation. Also, I am still amazed at the skills of especially Mr. Matti Savela and Mr. Jarmo Ruusila, without whom I could not have built my reactor. I thank them both!

I am also grateful to Dr. Pentti Saarenrinne, Dr. Markus Honkanen and Mr. Antti Laakso for their excellent expertise in the field of PTV measurements.

I am deeply indebted to Dr. Evgeny Podkletnov and Mr. Janne Wahlman for their altruistic work in helping me to conduct the measurements. I would also like to mention Mr. Ilkka Saarenpää and Miss Merja Tokola for their work on this project and Mrs. Johanna Heikkinen for conducting TGA analyses.

I would like to thank Matti Rautanen, Pertti Petänen, Jouni Kinni, Vesa Wallen, Ilkka Anttila, Ari Kokko, Tero Luomaharju, Riku-Ville Nurminen and Markku and Juha Roppo for their help, understanding, support and encouragement during the course of this work. Special thanks are due to Mr. Matti Ylitalo for his brilliant ideas and CFD modeling and to Ari Saario, Jaani Silvennoinen, Hannu Koskela and Pekka Arhenius for their help in preparing journal materials.

Warm thanks are due to Professors Antti Oksanen, Reijo Karvinen and Pertti Martikainen and to Mr. Jaakko Silpola for their professional advice during this project. I would also like to thank Mr. Danny Donoghue for reviewing the English of the manuscript.

Friends have encouraged and helped me a lot. I express warm thanks to all of them. Especially I would like to mention Mr. Pauli Haukka for being a brilliant jack-of-all-trades and thank him for his work in keeping Team Rusina® going. Furthermore, I would like to thank Mr. Kai Savolainen for his amazing stories. Do not believe all that is written in internet! Also, I would like to thank all the members of Soittorasia, Shinasu and Frozen Dawn for an excellent time. I wish you all the best of luck.

I also wish to extend my deepest thanks to my family. I owe more than I can express with words to my mother Aila and my father Heikki and especially to 'Amma' and Ate Huusko. I also owe my warmest thanks to my brothers Simo, Sami and Riku-Petteri as well as to my sister Rosa-Maria. I am not forgetting you, Risto and Jyrki Jokinen. Thanks are due to you, too. I would also like to thank Pirjo and Seppo Tammikari for their support.

The greatest gratitude is due to my wife Jonna, to my son Joonas and to my daughter Elina. Doing this work has certainly required a lot of adjustments on your part, but knowing I have your love and support has carried me through it. Life is not worth living and no fuel is worth pyrolysing without you.

Tampere, April 2007

Jani Lehto

Contents

Nomenclature

Symbols

A	1. Frequency factor	s^{-1}
	2. Area	m^2
A_p	Surface area of the particle	m^2
A_{pi}	Projected area of the particle image	m^2
$\tilde{A}$	Projected area of the body normal to the flow	m^2
B	Transpiration number	-
Bi	Biot number	-
C_D	Drag coefficient	-
$\dot{C}_s''$	Heat capacity flux of volatiles from particle surface	$Wm^{-2}K^{-1}$
c	Specific heat capacity	$Jkg^{-1}K^{-1}$
d	Diameter	m
E	Activation energy	$Jmol^{-1}$
E_0	Mean activation energy	$Jmol^{-1}$
g	Acceleration of gravity (=9.81)	ms^{-2}
h	Heat transfer coefficient	$Wm^{-2}K^{-1}$
k	Reaction rate constant	s^{-1}
M	Molar weight	$gmol^{-1}$
m	Mass	kg
$\dot{m}''$	Mass flux	$kgm^{-2}s^{-1}$
Nu	Nusselt number	-
Nu_0	Nusselt number calculated without Stefan flow	-

n	Order of the reaction	-
Pr	Prandtl number	-
Py	Pyrolysis number	-
Py'	Pyrolysis number for external heat transfer	-
p	Circumference of a particle image	m
q_{pyr}	Reaction enthalpy of the pyrolysis reactions	Jkg^{-1}
R	Particle's distance from the reactor centreline	m
Re	Reynolds number	-
R_u	Universal gas constant (=8.314)	$Jmol^{-1}K^{-1}$
R_0	Radius of the reactor	m
r	Radius of the particle	m
S	Shape factor	-
T	Temperature	K
t	Time	s
V	Mass fraction of volatiles released by time t	-
V_c	Mass fraction of volatiles left in the char	-
V_p	Volume of the particle	m^3
V_{prox}	Amount of volatiles from the proximate analysis	-
V^*	Mass fraction of volatiles released at $t=\infty$	-
v	Velocity	ms^{-1}
X	Conversion	-
X_{corr}	Correction factor	-
y_1	Volatile release in the low-temperature reactions	-
y_2	Volatile release in the high-temperature reactions	-

Δm_{silo}	Weight loss of the fuel silo	kg

Greek letters

α	Element specific coefficient	m^3kmol^{-1}
ε	1. Porosity	-
	2. Emissivity	-
λ	Thermal conductivity	$Wm^{-1}K^{-1}$
θ	Correction factor	-
ρ	Density	kgm^{-3}
σ	1. Standard deviation	-
	2. Stefan-Boltzmann constant (= 5.67×10^{-8})	$Jm^{-2}s^{-1}K^{-4}$
τ	Characteristic time	s
τ_R	Time constant of chemical reaction	s
τ_T	Time constant of thermal heat conduction	s
μ	Dynamic viscosity	$kgm^{-1}s^{-1}$
γ	Mass fraction	-

Subscripts

act	Unreacted(=’active’) fuel
ash	Ash
ave	Average
c	Char
daf	Dry ash-free fuel particle
E	Einstein
eff	Effective
g	Gas

i	Species i
mea	Measured
o	Outer
p	Particle
pore	Pore
r	Ratio
rad	Radiant
S	Solid
s	Surface of the particle
sph	Spherical
T	True (moisture and ash included)
t	True (dry ash-free)
vol	Volatile compounds
w	1. Water
	2. Reactor wall
∞	After pyrolysis, final
0	Initial
1	Reaction 1
2	Reaction 2

Superscripts

act	Un-reacted(=’active’) fuel
c	Char
0	Initial
*	Corrected

Abbreviations

ANN	Artificial Neural Network
BFB	Bubbling Fluidized Bed
CFB	Circulating Fluidized Bed
CFD	Computational Fluid Dynamics
CHP	Combined Heat and Power
CPD	Chemical Percolation Devolatilization
DAEM	Distributed Activation Energy Model
DTR	Drop Tube Reactor
EFR	Entrained Flow Reactor
FB	Fluidized Bed
FG-DVC	Functional-Group, Depolymerisation, Vaporisation, Crosslinking
FTIR	Fourier Transform Infrared Spectroscopy
HWM	Heated Wire Mesh
LFRD	Laminar Flow Reactor Developed in this work
MP	Milled Peat
IPCC	Intergovernmental Panel of Climate Change
PF	Pulverized Fuel
PIV	Particle Image Velocimetry
PSD	Pine Saw Dust
PTV	Particle Tracking Velocimetry
R	free Radical groups
TGA	ThermoGravimetric Analysis
TUT	Tampere University of Technology

CHAPTER 1

Introduction

Due to increased environmental awareness, interest concerning the impact of energy production on the environment has increased all over the world. The utilization of biomass in combustion processes instead of fossil fuels, such as oil and coal, is an effective way to reduce greenhouse gas emissions. However, renewable fuels, such as peat and biomass, have different combustion characteristics than those of fossil fuels. Therefore, knowledge gathered from fossil fuels cannot directly be applied to renewable fuels.

This dissertation deals with the pyrolysis of high-volatile-content fuels. The main focus is on the pyrolysis of peat, which is an important slowly renewable energy source, especially in the Nordic Countries. In this chapter, the role of peat as an energy source is discussed. Also, the basic concepts of co-combustion and fluidized bed technologies are briefly introduced. Finally, the aim and the structure of this dissertation are explained.

1.1 Energy from peat and biomass

The pulp and paper industry has been the forerunner in the use of biomass as a fuel. Biomass combustion became common in the 1980s when the pulp and paper industry and sawmills started to utilize the energy contained in the by-products from their main process, i.e. bark, wood residues and sawdust, in fluidized bed boilers (Kokko and Nylund, 2005). Earlier, grate-fired boilers were used for biomass firing, but when different types of biomass with varying properties started to be burned simultaneously, fluidized bed combustion increased its market share at the expense of grate firing (Kinni et al., 2005)(Kokko and Nylund, 2005). Fluidized bed boilers are more flexible in terms of fuel moisture and fuel type, and have better efficiency and lower emissions than grate-fired boilers.

However, since process by-products cannot cover all of the steam requirements of a pulp and paper mill, outside fuels are needed. Earlier, oil and gas were used as supplementary fuels, but recently local and cheaper fuels such as wood and peat (Confederation of Finnish Industries, 2004) have replaced the expensive gas and oil as supplementary fuels.

Furthermore, in the Nordic Countries, where Combined Heat and Power production (CHP) is common, a big proportion of district heating is produced by burning forest fuels and peat. For example in the year 2005, 28% of the district heating and CHP in Finland was produced by burning wood and peat (Finnish Energy Industries, 2006). Biomass-fired condensing power plants have increased in popularity due to government subsidies for green energy in Europe and USA.

1.2 Peat as energy source

Peat is a material formed from the partial decomposition of dead plants under wet, acidic conditions. It is usually found in un-drained stagnant areas called bogs, fens or mires. Natural peatlands accumulate carbon and nitrogen. Peatlands also affect global climate by binding carbon dioxide (CO_2) and releasing methane (CH_4) to the atmosphere (Minkkinen et al., 2002). Left in their natural state, peatlands produce large amounts of methane gas (Nykänen et al., 1998) , which is a greenhouse gas having 21 times the impact of carbon dioxide on the world's atmosphere.

One of the principal types of peat is moss peat, which is used as a main component of different growing media in horticulture, animal husbandry and agriculture for poultry and stable litters, as mulch and as an acidifying agent. It is also used in industry as an insulating material. Another type of peat is fuel peat, which is most widely used in the Nordic Countries, Ireland and parts of Russia.

During the last decade the pressure to reduce greenhouse gas emissions in energy production has increased since nearly all man-made CO_2 emissions are due to thermal conversion processes. In the still on-going debate concerning the

environmental impacts of energy production, the peat industry has been on the losing side since peat has been classified as a fossil fuel until recently.

This fossil fuel classification was strongly opposed, especially in Finland, which has the highest proportion of wetlands in terms of national area of any nation in the world, as it does not take into account the annual growth of peat and the possibility of producing biomass on cut-over peatlands (Sopo, 2001). The Finnish Ministry of Trade and Industry prepared a report called “The Role of Peat in Finnish Greenhouse Gas Balances”, in which it is stated that peat can be regarded as a slowly renewable natural resource. In the spring of 2006 the Intergovernmental Panel of Climate Change (IPCC) removed peat from the list of fossil fuels and added it to its own category called "peat". Recently, in December 2006, the European Parliament adopted a new “Resolution on a strategy for biomass and biofuels (2006/2082(INI))”. In item 78, it “calls on the Commission to include peat, with regard to the life-cycle aspect, as a long-term renewable energy source for biomass and bioenergy production”.

According to the recent research done by the Geological Survey of Finland, the top layer of the peatland which is younger than 300 years should be equated with wood-based fuels in energy economics (Mäkilä, 2006). Furthermore, the utilisation of forestry-drained peatland in energy production causes a lower climate impact than producing the same amount of energy with coal if the utilisation of renewable biomass (wood, reed canary grass) produced in the after-treatment of peatland is taken into account within a 100-year time horizon (Kirkinen et al., 2007). The CO_2 emissions from fuel peat combustion, produced at the beginning of the life cycle of peatland utilisation, have a significant influence on the climate. On the other hand, when peat is exploited, the peatland area can be used for producing carbon dioxide neutral fuel, either wood or reed canary grass, which lowers the total climate impact of peatland in relation to the produced energy (Kirkinen et al., 2007).

In Finland, as well as in other countries where peat has an important role in energy production, great interest is paid to the process of peat classification in terms of greenhouse gas emissions and emission trading.

For a researcher, peat is a very interesting fuel. It is an “intermediate” fuel, having attributes midway between those of highly volatile coals and biomass. Compared to coal, both peat and biomass fuels are characterized by low calorific values and by their high moisture and volatile content and different ash composition, which needs to be taken into account when dimensioning a boiler for burning peat and/or biomass. The biomass moisture varies during the year and also the ash characteristics vary greatly, depending on the origin of the material (Kinni et al., 2005).

1.3 Co-combustion

The idea of co-combustion is to replace some of the fossil fuels used in power plants with renewable ones. The co-combustion of coal and biomass has several advantages. First of all, a boiler capable of burning several different fuels has good fuel flexibility, which gives the owner a significant opportunity to minimize fuel costs (Kokko and Nylund, 2005). Furthermore, coals usually have a high sulphur content, whereas biomass have a low sulphur content, if any. When some of the coal is replaced by biomass, limestone consumption is lower and therefore reduces the operational cost (Kokko and Nylund, 2005). Vice versa, even a small amount of coal used together with biomass reduces the tendency towards corrosion and fouling.

The most substantial economic advantage of co-firing, now that emission trading has been started, is that the burning of biomass, either alone or with other fuels, reduces net CO_2 emissions. Biomass and other organic fuels are considered to be CO_2-neutral as the growing of biomass captures the same amount of CO_2 that is released during thermal conversion. Co-incineration of biomass and waste-derived fuels is also in compliance with the tightening directives to enhance recycling and minimize wasteland filling (Heikkinen, 2005).

1.4 Fluidized bed technology

Fluidization is a condition in which solid particles are suspended in an upward-moving gas stream so that the gas-solid particle mixture behaves like a fluid. In combustion processes, fluidization results in an expanded combustion zone with high turbulence, intimate solids-to-gas contact and a high heat transfer rate within the bed. Stable combustion is attained also with high-moisture fuels due to the high heat capacity of the bed. The bed temperature, normally between 750^{o}C and 950^{o}C, depends on the quality and amount of the fuel in the bed.

Two different fluidized bed combustion methods exist, i.e. Bubbling (BFB) and Circulating Fluidized Bed (CFB). These two combustion methods differ from each other in fluidization velocity. In BFB combustion, the fluidization velocity is typically around 1 m/s and the gas velocities in the furnace usually vary between 3 and 5 m/s. In CFB combustion, the fluidization velocity can be as high as 3 m/s and gas velocities in the furnace typically vary from 4 to 6 m/s. In a BFB, bed material stays in the lower furnace area, whereas in CFB combustion bed material fills the whole furnace and is returned to the bed by separate cyclone(s).

1.4.1 Bubbling fluidized bed combustion

In a BFB boiler the combustion takes place in a dense fluidized bed and directly above the bed. Small fuel particles are burned rapidly above the fluidized bed, which is mainly composed of sand with a small percentage of fuel and ash, while larger particles filter into the bed, where they are dried and gasified. Residual char is burned mainly in the fluidized bed, while volatile gases burn both in the bed and in freeboard above it.

BFB boilers can burn low-rank and low-quality fuels and have the best flexibility in terms of the variety of high-moisture fuels they can accept (Kinni et al., 2005). Other advantages of BFB combustion include high availability, reduced investment costs compared to CFB, high combustion efficiency and low emissions (Oka, 2004). Some typical operating values of BFB boilers are presented in Table 1.1

Table 1.1. Some typical operating values of BFB boiler.

Parameter	*Range*
Fluidizing velocity	0.7 - 2 m/s
Bed height	0.4 - 0.7 m
Temperature of primary air	20 – 400°C
Temperature of secondary air	20 – 400°C
Bed temperature	750 – 950°C
Freeboard temperature	700 – 1200°C
Secondary air proportion	30-70 %
Air ratio	1.1 – 1.4

1.4.2 Circulating fluidized bed combustion

The CFB process provides excellent conditions for the burning of several different fuels in the same boiler, which has been almost impossible with earlier technologies. Bed material circulation and high turbulence in the combustor ensure good mixing of the fuel and combustion air. An efficient particle separator, the cyclone, is the heart of the process. The cyclone separates the particles (including sand, limestone and un-burned fuel) from the flue gas and returns them to the bottom of the furnace via the loopseal located in the bottom of the cyclone.

Other significant benefits of CFB combustion are the possibility to efficiently remove sulphur from flue gases by injecting limestone into the furnace, low NO_X and CO emissions, efficient heat transfer inside the furnace and high combustion efficiency (Kokko and Nylund, 2005).

1.5 Objectives of the dissertation

In order to build reliable models for the combustion and gasification of peat and biomass, it is necessary to know the rate and the amount of volatiles released during devolatilization in conditions close to those in practical application. Devolatilization and combustion of the generated char are consecutive steps in combustion. As stated by Ulloa et al. (2004), devolatilization not only affects ignition and flame stability phenomena, but also determines the physicochemical characteristics of the generated char, which in turn strongly affect its reactivity during the combustion step.

The combustion of released volatiles is a fundamental part of the combustion process of peat and biomass, whereas it does not have such a significant role in the combustion of coal. Indeed, it is possible to generalize the combustion process in the fluidized bed as the combustion of two different fuels, i.e. combustible volatiles and char, as stated by Oka (2004). Of course in reality the situation is not that simple.

It is known that several factors, such as temperature and heating rate, have a strong effect on the volatile yield of a fuel during devolatilization. Usually, the volatile content of a fuel is determined using standardized slow heating rate tests developed for coal or using thermogravimetry. These methods give an idea of the volatile content of low-volatile-content fuels like coal, but these tests do not work reliably with high-volatile-content fuels like peat and biomass. As a result, the test methods developed for coal and the results obtained from research on the pyrolysis and combustion of coal cannot directly be adopted to peat and biomass cases.

At the moment, no standard method exists for determining the volatile content of biomass fuels.

The objectives of this dissertation were:

- To develop and characterize a laboratory-scale test reactor for reliable determination of the volatile content of high-volatile-content fuels like peat and biomass in conditions similar to those of fluidized bed boilers.
- To compare different methods to determine volatile matter content with the laminar flow reactor developed in this work (LFRD).
- To measure the volatile yield of Finnish milled peat at different residence times in the LFRD.
- To calculate the kinetic parameters for Finnish milled peat from experimental data using different kinetic models describing the pyrolysis phenomenon.
- To present a method for estimating final volatile yield of peat pyrolysis.

1.6 Methology

This work is intended to provide help in understanding the pyrolysis phenomena of high-volatile-content solid fuels, particularly peat, in conditions similar to those in fluidized bed boilers. To achieve this, fundamental experimental and modeling tools were used:

- Volatile content of Finnish milled peat and pine sawdust were determined using standardized methods, thermogravimetry and the LFRD.
- Optical methods were used for characterization of the LFRD and for studying the properties of peat used.
- The LFRD was used for determining the volatile yield of Finnish milled peat at different temperatures and at different residence times.
- Modeling tools were used for calculating the kinetic parameters from experimental data.

1.7 Contribution

In this dissertation, a laboratory-scale laminar flow reactor which is well-suited for determining the volatile content of high-volatile-content fuels is introduced and characterized. Furthermore, it was discovered that the LFRD provided highest volatile yields for Finnish milled peat and pine sawdust fuels when it was compared to other common analysis methods.

The LFRD was used to determine the volatile yield of Finnish milled peat at different residence times in the reactor in conditions similar to those in a fluidized bed boiler. Based on the experimental results, the kinetic parameters for Finnish milled peat are presented using two different kinetic models. Furthermore, a simple and straightforward method is introduced for determining those parameters from experimental data. Finally, a method for estimating final volatile yield of peat pyrolysis is presented.

In the modeling part of the work, it is demonstrated that in drop tube reactors the drag coefficient of the fuel can be a major source of error. Therefore, it is proposed that this case-specific factor should be measured for every fuel tested. For example, optical measurement techniques can be used for this purpose, as presented in this dissertation.

1.8 Structure of the dissertation

This dissertation is constructed as follows. In Chapter 2 theory and models of pyrolysis are introduced and discussed. In Chapter 3 some commonly used laboratory-scale analysis methods used for solid fuel characterization are presented, while Chapter 4 deals with the characterization of the reactor and reports the results of pyrolysis experiments. Chapter 5 presents the pyrolysis modeling results. Finally, based on the experimental and modeling work, conclusions from the present work and recommendations for further work are given in Chapter 6.

CHAPTER 2

Pyrolysis

The combustion and gasification of a fuel particle can be divided into different stages. According to Saastamoinen (2002), a particle is first heated to the dehydration temperature. After the dehydration stage, the particle goes through the devolatilization, gasification or char combustion phase and for big particles these stages might be partly overlapping. During the devolatilization stage, the volatile matter contained in the solid fuel is released due to thermal decomposition, forming gas and tar compounds. Usually, the volatile matter of an organic fuel comprises the major part of the fuel's mass, hydrogen, oxygen, nitrogen and sulphur content. The amount and chemical composition of the gas formed, as well as the reactivity of the residual char, are dependent on the final temperature of the particle, heating rate, particle size, properties of the fuel and gas medium, and somewhat on the surrounding pressure. Even though the devolatilization stage is very short compared to the duration of the total gasification or combustion stages, it has a great effect on the overall efficiency of the gasification or combustion process (Saastamoinen, 2002). When devolatilization is carried out under inert conditions, it is termed pyrolysis. Furthermore, if the pyrolysis takes place at a rapid heating rate, it is termed flash pyrolysis.

In this chapter, the theory behind pyrolysis is discussed. Also, some correlations for important fuel thermal properties are introduced.

2.1 Pyrolysis mechanism

Pyrolysis is a very complex phenomenon. It is dependent on the chemical, structural and physical properties of the fuel particle, which change in the course of pyrolysis. Due to the complexity of the process, a complete description of

pyrolysis is not yet possible. Therefore, based on experimental results, many different mechanisms and models have been proposed.

Pyrolysis reactions start after the dehydration stage when the temperature level is high enough for chemical reactions to commence with the rupture of bonds. According to Saxena (1990), pyrolysis begins with the cracking of bridges between the ring systems, resulting in the formation of highly reactive free radical groups (R), such as $–CH_2-$ and -O-. Since polynuclear aromatic compounds diffuse slowly even at high temperatures, they start to condense with the elimination of hydrogen. The ultimate product due to the condensation reactions is char. In addition, at high temperatures, CO is also produced by the cracking of heterocyclic oxygen groups. The following typical reactions take place in stages as temperature is increased (Saxena, 1990):

Cracking: $R\text{-}CH_2\text{-}R \rightarrow R\text{-}R' + \text{-}CH_2$ (2.1)

Saturation: $\text{-}CH_3 + H' \rightarrow CH_4$ (2.2)

$\text{-}OH + H' \rightarrow H_2O$ (2.3)

Tar production: $\text{-}R\text{-}CH_2 + H' \rightarrow R\text{-}CH_3$ (2.4)

Condensation reaction: $R\text{-}OH + H\text{-}R \rightarrow R\text{-}R + H_2O$ (2.5)

$R\text{-}H + H\text{-}R' \rightarrow R\text{-}R' + H_2$ (2.6)

In addition, oxides of carbon are produced by the reaction

$R\text{-}COOH \rightarrow R\text{-}H + CO_2$ (2.7)

The hydrogen in fuel is used up to partly produce hydrocarbons and water, and is partly liberated as molecular hydrogen. However, pyrolysis always produces tar and char due to the inefficient use of intrinsic hydrogen (Saxena, 1990).

As the pyrolysis gases formed go through the porous carbon matrix to the surface, some secondary reactions may occur, either heterogeneously in the fuel particle or homogeneously in the gas phase. During these secondary reactions, volatiles usually degrade to lighter gaseous compounds.

The volatiles change the heat transfer environment of the surface of the fuel particle and slow down heat conduction inside the particle (Saxena, 1990). In an oxygen-rich atmosphere, also the combustion of released volatiles affects devolatilization. Furthermore, Pyle and Zaror (1984) pointed out that it is possible for gases to diffuse to the colder part of the particle and condense in the un-reacted part of the fuel.

The heat and mass transfer processes and chemical kinetics greatly affect pyrolysis. In different circumstances one of the processes might be slower than others and therefore control the rate of pyrolysis. Pyrolysis of a small particle (<100 μm) is usually isothermal and kinetically controlled. On the other hand, pyrolysis of a large particle (>100 μm) is significantly different from that of a small particle, due to the relative importance of the heat and mass transfer resistances. The resistances not only affect the volatile release rate, but also the product yield and distribution (Saxena, 1990) (Solomon et al., 1992).

The characteristics of overall weight loss are rapid initial release of about 80-90 % of the volatiles, followed by slow release of the remaining 10-20 % (Solomon et al., 1992) (Bharadwaj et al., 2004). This behaviour has been referred to as the two-component hypothesis of pyrolysis (Solomon et al., 1992).

2.2 Pyrolysis products

Pyrolysis gas products can be divided into two groups, i.e. gases and tars. Product gases usually consist of permanent gases at room temperature, such as CO_2, CO, CH_4, H_2, H_2O, C_2H_6, C_2H_4, C_2H_2, C_6H_6 and many compounds consisting of sulphur and nitrogen, such as COS, HCN and NH_3. Differentiating char from tar is more complicated. The lightest fragments of the decomposing

macromolecular network evolve as tar. In the following, tars are defined as heavy hydrocarbons which are gaseous under pyrolysis conditions but condense at room temperature (Saxena, 1990) (Solomon et al., 1992) (Yu et al., 1997). The remaining solid is called char.

In general, pyrolysis water, CO_2 and tar evolve at lower temperatures, whereas hydrocarbons, CO and hydrogen evolve at higher temperatures. Methane is an intermediate species which overlaps both regimes and appears to derive from multiple sources (Saxena, 1990) (Solomon et al., 1992). According to the research done by Yu et al. (1997), benzene is the dominating tar component at all temperatures.

Temperature influences the primary decomposition reactions as well as the secondary reactions of the escaping volatiles. Higher pyrolysis temperature affects the composition of the gaseous products and promotes their formation at the expense of total tar (Yu et al., 1997). Temperature also influences the composition of tar and char from pyrolysis (Zanzi et al., 1996). At higher temperatures, the char contains less hydrogen and oxygen since these are given off as volatiles. The total sulphur content of char decreases with temperature. The yield of a given volatile compound increases with increasing temperature. However, the amount of each substance produced will be different at different temperatures (Saxena, 1990).

Pyrolysis at high pressures produces more char, less tar and more hydrocarbons. However, an investigation carried out by Holst et al. (1991) in the pressure range of 10-40 bar in inert conditions showed that pressure only slightly influenced the product composition. Particle size has an almost identical effect on product distribution as pressure has, due to the more extensive secondary reactions which play an increasingly more important role as particle size increases (Saxena, 1990).

The chemical composition of the fuel also influences the distribution of pyrolysis products. High carbon and low oxygen content of the fuel and low H/C ratio favours higher yields of char (Saxena, 1990).

2.3 Factors affecting pyrolysis yield

The amount of volatiles released during pyrolysis is strongly dependent both on the temperature level and the residence time at peak temperature. In general, the higher the temperature level, the more volatiles are released. Also, the number of secondary reactions is increased with higher temperature level, which usually leads to a decreased amount of tar and increased amounts of volatiles and char. Secondary reactions are mainly connected with the highly reactive and unstable tar compounds which are formed during pyrolysis.

If there are no secondary reactions, the peak temperature and the residence time at peak temperature affect more the amount of volatiles released than the heating rate. However, it is usually difficult to separate the effect of heating rate and the effects of peak temperature and residence time at peak temperature. As the heat flux is proportional to the temperature difference between the particle and the environment, at higher temperatures the heating rate, which is proportional to heat flux, is higher. The heating rate influences the time-temperature history of pyrolysis and therefore it affects the cumulative yield and rate of devolatilization at a given temperature (Saxena, 1990) (Zanzi et al., 1996) (Shuangning et al., 2006).

The stronger effect of the heating rate on the formation of char from biomass than on the formation of char from coal has been reported for example by Zanzi et al. (1996). When they compared the pyrolysis of coal and biomass, the biomass samples produced more volatiles. According to Zanzi et al. (1996), this may be attributed to the higher reactivity of the biomass, which is due to the high amount of cellulose in biomass. Rapid heating rate favours the depolymerization of cellulose and the formation of volatiles as the residence time of biomass at temperatures below 300°C is insignificant. At this temperature dehydration

reactions and the formation of less reactive anhydrocellulose favour char formation. Furthermore, Li et al. (2004) reported that flash pyrolysis of biomass produced more volatiles than slow pyrolysis at the same temperature level.

Zanzi et al. (1996) also found that rapid devolatilization of the fuel favours the formation of char with high porosity and high reactivity. Furthermore, they reported that for a certain biomass and for a certain particle size, a high enough heating rate is reached at a certain temperature. Further increase in heating rate because of an additional increase in temperature does not affect the char yield (Zanzi et al., 1996).

If the pressure is increased, the residence time and concentration of volatiles within a particle is increased. This results in more secondary reactions of certain reactive species, like tar. On the other hand, some secondary reactions, like cracking, decrease the amount of volatiles released (Saxena, 1990). Research done by Cetin et al. (2004) showed that char reactivity increases with increasing pyrolysis rates and decreasing pyrolysis pressure. They also reported that pressure was also found to influence the physical and chemical structures of char particles. The effect of surrounding pressure is more significant for fuels which contain lots of heavy tar molecules (Cetin et al., 2004).

Particle size affects both the thermal response and the extent of secondary reactions. As particle size increases, the heating rate decreases. Also, the residence time of volatiles within the particle increases, which leads to an increased amount of secondary reactions. The effect of particle size is more significant for fuels which contain lots of volatile matter (Saxena, 1990) (Solomon et al., 1992).

Pyrolysis tests are normally carried out in inert conditions, in which case gasification reactions in residual char do not usually occur. Nonetheless, volatiles contain water vapour and carbon dioxide, which might gasify the residual char if the residence time of the gases inside the particle is long enough (Järvinen, 2002).

2.4 Factors controlling rate of pyrolysis

Depending on the fuel properties and the surrounding environment, the rate of pyrolysis is controlled by one or more of the following processes:

- Heat transfer from hot surroundings to a particle (external heat transfer).
- Heat conduction inside a particle (internal heat transfer).
- Time required for chemical reactions (chemical kinetics).
- Mass transfer of volatiles through a particle.

In general, particle size is the most important factor when determining the rate of pyrolysis. It is commonly agreed that for small coal particles (< 100 μm) the time required for heat and mass transfer is much shorter than the time required for chemical processes, in which case the chemical kinetics control the rate of pyrolysis (Bharadwaj et al., 2004) . However, mass transfer can be considered to account for some variations in volatile yields of pyrolysis tests due to the possible secondary reactions. As particle size increases, the time required for heat and mass transfer increases until these processes are so slow that chemical kinetics are no longer controlling the rate of pyrolysis. Fuel thermal properties, porosity and behaviour under pyrolysis conditions are the main factors affecting the heat and mass transfer (Saxena, 1990).

2.4.1 Mass transfer

Mass transfer has an effect on both product yield and product evolution rates. The effect of mass transfer on the kinetics of gaseous volatile evolution is unimportant for small or very porous particles. However, when observing the fast pyrolysis of compact fuels, the time required for mass transfer might be of the same order as the time required for chemical reactions. Additionally, the fast release of volatiles may break down very compact fuel particles, like coal. The rate of mass transfer is significant when observing fuels which form lots of tars during pyrolysis. The diffusion of large tar molecules is usually slow, and during

the diffusion large molecules may break down to smaller molecules, in which case the mass transfer resistance is smaller (Saxena, 1990) (Solomon et al., 1992).

Mass transfer is controlled by internal and external resistances. Assuming isolated particles, the gas flow out of a particle is controlled by the mass transfer resistance of the particle‘s external boundary layer. If particles are not isolated (i.e. if they are in a thick bed), the transport through the entire bed might be controlling transport resistance. The mass transfer inside the particle is a result of hydrodynamic flow or diffusion and according to Solomon et al. (1992) the transport resistances might involve the following mechanisms:

- Transfer through the pores.
- Transfer of bubbles through melt phase.
- Transfer of tars to bubbles or pores.

However, it is often not clear which of the above possibilities govern behaviour in any particular situation.

To summarize, while the mass transfer may affect the product distribution and yields and may have a limited affect on the kinetics of higher heating rate experiments, it does not normally control the rate of pyrolysis of small or porous particles (Solomon et al., 1992). However, it affects the gasification and burning of a particle as the gas flow out of the particle may prevent the oxygen or gasification gas from entering the particle (Biagini et al., 2005).

2.4.2 Heat transfer and chemical kinetics

The internal heat transfer of a particle consists of conduction in porous material. The convective and radiant heat transfer mechanisms constitute the external heat transfer. The relative importance of these heat transfer mechanisms can be studied using the heat transfer Biot number *Bi* (Pyle and Zaror, 1984) (Saxena, 1990):

$$Bi = \frac{h_o r_p}{\lambda_p} \tag{2.8}$$

where h_o is the outer heat transfer coefficient, r_p is the radius of the particle and λ_p is the thermal conductivity of the particle.

When the Biot number is small (*Bi* << 1), the internal heat transfer is so fast that the particle can be assumed to be practically at a uniform temperature and pyrolysis takes place evenly in the whole particle. In that case, the rate of pyrolysis is controlled either by external heat transfer or chemical kinetics. On the other hand, when the Biot number is big, external heat transfer is quicker than internal heat transfer and there are significant temperature gradients inside the particle (Pyle and Zaror, 1984).

The relative importance of internal processes can be studied by comparing the time constants of the pyrolysis reaction τ_R and heat conduction τ_T. The ratio of these time constants is called the pyrolysis number *Py*:

$$Py = \frac{\tau_R}{\tau_T} = \frac{1/k}{\rho_p c_p r_p^{\,2} / \lambda_p} = \frac{\lambda_p}{\rho_p c_p r_p^{\,2} k} \tag{2.9}$$

in which ρ_p is the density of the particle, c_p is the specific heat capacity of the particle and *k* is the reaction rate constant.

If *Py* >> 1, reaction is slow compared to thermal heat conduction, and both chemical kinetics and internal heat transfer must be taken into account. On the

other hand, if *Py* << 1, chemical reaction is very fast and the heat transfer inside the particle controls the rate of pyrolysis (Pyle and Zaror, 1984).

When a pyrolysis number for external heat transfer *Py'* is introduced, the controlling factor for pyrolysis can be evaluated for a situation where there are no temperature gradients in the particle (Pyle and Zaror, 1984):

$$Py' = Bi * Py = \frac{h_o}{k\rho_p c_p r_p} \tag{2.10}$$

When *Py'* is high, the rate of pyrolysis is controlled only by chemical kinetics and the particle and the surroundings are at a uniform temperature, which means that particle size does not affect the rate of pyrolysis. On the other hand, if *Py'* is small, the reaction rate is so high that the external heat transfer to the particle controls the rate of pyrolysis and thus the particle size affects the rate of pyrolysis. Table 2.1 summarizes the results (Pyle and Zaror, 1984).

Table 2.1. Summary of factors controlling rate of pyrolysis.

Controlling factor	*Bi*	*Py*	*Py'*
Chemical kinetics	Small		Large
External heat transfer	Small		Small
Internal heat transfer	Large	Small	

Peat and biomass particles are usually very porous, which results in the heat transfer in a particle being relatively slow. In contranst, the mass transfer in peat and biomass particles is usually fast, in which case it does not control the rate of pyrolysis.

2.5 Chemical kinetics of pyrolysis

During pyrolysis, hundreds of different chemical reactions take place and the exact modeling of these reactions is neither possible nor practical. In fact, the total amount of volatiles, the different products and the rates of production are more interesting than single chemical reactions. The literature presents several different models for describing the chemical kinetics of pyrolysis. These models do not necessarily describe the physical and chemical phenomenon correctly, but they correlate with the experimental results.

The temperature dependence of the chemical reactions is normally described by the Arrhenius expression (Holst et al., 1991) (Saastamoinen, 2002):

$$k = A \exp\left(\frac{-E}{R_u T}\right) \tag{2.11}$$

Consequently, the kinetic parameters usually refer to the activation energy (*E*) and frequency factor (*A*) in the Arrhenius expression.

In theory, the activation energy is the amount of energy needed to start the chemical reactions. Furthermore, the frequency factor is the maximum reaction rate constant for the situation where all collisions between molecules initiate a chemical reaction. The exponential form of the activation energy in the Arrhenius equation describes the fraction of the collisions in which the collision energy is higher than the activation energy. Therefore, the product of the exponential part and the frequency factor describes those collisions that could initiate a chemical reaction. Thus, the activation energy determines the temperature level needed for pyrolysis reactions to start.

Kinetic parameters are normally solved from experimental test results. A pyrolysis model which uses a certain set of kinetic parameters is often valid only for a limited temperature and heating rate level. If the kinetic parameters correlate well with the experimental data, it might be possible to extrapolate the model to wider temperature and heating rate levels.

However, for the same fuels, several different kinetic parameters have been presented in the literature. Due to that fact, many different possible explanations for such discrepancies have been put forward. First of all, the fuel samples often differ widely and are themselves heterogeneous (Solomon et al., 1992). On the other hand, as stated by Saastamoinen (2002), discrepancies are commonly due to the obscurity of the particle temperature history during experiments and due to uncertainty in determining the particle residence time. In the majority of cases, particle temperature determination is the main reason for these variations.

For pyrolysis experiments, the test conditions should be designed in such a way that the effects of heat and mass transfer are clearly known, especially if direct particle temperature measurement is not possible. However, the reaction enthalpies of pyrolysis are usually so small that they do not have a significant effect on the temperature of the particle.

2.6 Kinetic models

In independent reaction models, such as single first-order and distributed activation energy models, the fuel is assumed to be composed of a set of different components which decompose independently through first-order reactions. In competing reaction models, it is assumed that there are several different temperature-dependent reaction paths and that the fuel is decomposed through one of these. In any of these models, no actual chemical structures or equations are used and it is assumed that components go through simple stochiometric reactions.

Network models are phenomenological models which consider fuel as a macromolecule. During pyrolysis, the macromolecular structure of the fuel disintegrates into volatile fragments (Niksa, 1995). Artificial neural networks which utilize large databases and ‘learning’ neurals could be the next generation of CFD models (Abbas et al., 2003).

2.6.1 Single first-order model

The simplest way of describing the chemical kinetics of pyrolysis is to use a single first-order model (one-reaction model). The model is based on the assumption that the rate of pyrolysis is proportional to the amount of volatiles left in the particle according to the equation (Saxena, 1990) (Saastamoinen, 2002):

$$\frac{dV}{dt} = k\left(V^* - V\right)^n \tag{2.12}$$

Here V^* is the mass fraction of volatiles released at $t=\infty$ and V is the mass fraction of volatiles released by time t. The order of the reaction n is usually assumed to be one, which means that the reaction is a first-order decomposing reaction.

The good point of the model is that only three experimental values are needed, i.e. the activation energy, the frequency factor and the final amount of volatiles (Saastamoinen, 2002). On the other hand, the inability to predict volatile yield is the biggest shortcoming of the model. Furthermore, pyrolysis usually takes place over a wide temperature range, which is very difficult to describe with only one activation energy value. In spite of these limitations, single first-order models are often used due to their simplicity.

2.6.2 Distributed Activation Energy Model (DAEM)

The DAEM is one of the most comprehensive models for analysing complex reactions such as pyrolysis of coal and biomass. It represents pyrolysis as a simultaneous occurrence of irreversible, independent and first-order decomposition reactions that describe the evolution of hypothetical n species during the pyrolysis. The pyrolysis rate of an i species is given by (Anthony et al. 1974)(Saxena, 1990)(Rostami et al., 2004) (Ulloa et al., 2004):

$$\frac{dV_i}{dt} = k_i\left(V^*_i - V_i\right) \tag{2.13}$$

The rate constants are given by the Arrhenius expression $k_i=A_i exp(-E_i/R_u T)$, E_i being the activation energy and A_i being the frequency factor for the pyrolysis of a species *i* (Saxena, 1990) (Ulloa et al., 2004).

Usually, it is further assumed that all reactions share the same frequency factor and thus the reactivity distribution is represented by a continuous distribution of activation energies. The DAEM assumes that the evolution of a given product involves an infinite number of independent chemical reactions (Rostami et al., 2004).

The fractional conversion X_i at any time *t* is obtained by integration of Equation 2.13 (Saxena, 1990)(Ulloa et al., 2004):

$$X_i = \frac{V_i}{V_i^*} = 1 - \exp\left[- \int_o^t k_i dt \right] \tag{2.14}$$

It is further assumed that the number of reactions is large enough to permit the activation energies to be expressed as a continuous distribution function *F(E)*, satisfying $\int_0^\infty F(E)dE = 1$.

According to Saxena, the peak in the *F(E)* curve corresponds to the tar formation reaction, the region with low activation energy corresponds to the formation of H_2O and CO_2, while the region of high activation energy corresponds to the formation of hydrocarbons, CO and H_2 (Saxena, 1990).

The total conversion (*X*) to volatiles at time *t* is given by (Saxena, 1990)(Rostami et al., 2004) (Ulloa et al., 2004):

$$X = \frac{V}{V^*} = 1 - \int_0^\infty \exp\left(\int_0^t - k dt \right) F(E) dE \tag{2.15}$$

Usually, *F(E)* is taken to be a Gaussian distribution with a mean activation energy of E_0 and a standard deviation σ, leading to (Saxena, 1990) (Rostami et al., 2004):

$$F(E) = \frac{1}{\sigma\sqrt{2\pi}} \exp\left(\frac{-(E - E_0)^2}{2\sigma^2}\right) \tag{2.16}$$

Using Equations 2.15 and 2.16, the solution for total volatiles becomes:

$$\frac{V^* - V}{V^*} = \frac{1}{\sigma\sqrt{2\pi}} \int_0^{\infty} \exp\left(-A\int_0^t \exp\left(\frac{-E}{RT}\right)dt - \frac{(E - E_0)^2}{2\sigma^2}\right)dE \tag{2.17}$$

However, as the DAEM is quite a complex model, it has been reported to be computationally expensive (Eaton et al., 1999). Furthermore, Ulloa et al. (2004) concluded that the assumption of Gaussian distribution may be questionable when activation energy values are widely distributed, in which case the frequency factor does not necessarily remain constant.

2.6.3 Two-competing-reactions model

In competing-reaction models, fuel is assumed to decompose via one of several possible reaction paths, depending upon the time-temperature history. In the two-competing-reactions model, the formation of volatiles and char is described by two reactions which compete for the remaining un-reacted fuel.

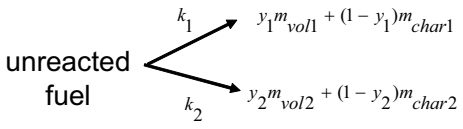

Figure 2.1. Thermal decomposition of fuel via two-competing-reactions model.

The two-competing-reactions model is given as (Kobayashi, 1972):

$$\frac{dm_{act}}{dt} = -(k_1 + k_2)m_{act} \tag{2.18}$$

$$\frac{dm_{vol}}{dt} = (y_1 k_1 + y_2 k_2)m_{act} \tag{2.19}$$

$$\frac{dm_c}{dt} = \left[(1 - y_1)k_1 + (1 - y_2)k_2\right]m_{act} \tag{2.20}$$

In Equations 2.18-2.20, m_{vol} is the mass of the volatiles, m_{act} refers to the mass of the un-reacted fuel at time *t,* m_c is the mass of the char and y_1 refers to the volatile release in low temperature reactions and it can, for example, be obtained from proximate analysis of the fuel.

Furthermore, y_2 refers to the volatile yield in high temperature reactions and it can, for example, be determined using the following equations (Jamaluddin et al., 1986):

$$y_2 = Q \cdot V_{prox} \tag{2.21}$$

$$Q = \frac{V^*}{V_{prox} - V_c} \tag{2.22}$$

where V_{prox} is the amount of volatiles from the proximate analysis and V_c is the mass fraction of the volatiles left in the char.

One of the advantages of this model is that it takes into account the dependence of volatile yield on the final temperature. When this model is used, the amount of char generated is dependent not only on the heating rate but also on the peak temperature (Saastamoinen, 2002).

2.6.4 Network models

Three fundamental, phenomenological network models have been developed for predicting the physical and chemical behaviour of coals during devolatilization, i.e. CPD (Grant et al., 1989), FG-DVC (Solomon et al., 1993b) and FLASHCHAIN (Niksa, 1995). The network models present the coal as a macromolecule consisting of clusters of aromatic rings connected by bridges of varying reactivity. According to Niksa (1995), the devolatilization process is presented as a depolymerization that changes the coal's macromolecular structure, leading to a breakup of existing bridges and the formation of new ones. Each model can predict yields and evolution rates of the main gaseous components, tars and char based on sample-specific characterization data. The main advantages of the network models are their ability to operate in a wide

range of different process conditions and their applicability to a wide range of coals. Network models have been successfully used to provide input data for CFD combustion sub-models (Brewster et al., 1995) (Backreedy et al., 1999) (Jones et al., 1999). Recently, the FG-DVC and FLASHCHAIN models have been expanded for use with biomass fuels.

2.6.5 Neural network models

During the past few years, the idea of using artificial neural networks (ANNs) also in combustion applications has gained attention. In general, ANNs are a collection of small individually interconnected computational units that implement simplified models (Abbas et al., 2003). According to Kalogirou et al. (2003), when implemented in computers, ANNs do not perform any specific tasks, but instead they are trained with respect to data sets until they learn patterns used as inputs. Once they are trained, new patterns may be presented to them for prediction or classification.

Instead of using physical and chemical equations to describe complex processes, ANNs use large databases from different experimental set-ups and are trained to retrieve the required rate constants for a particular application. The first results concerning combustion applications have been promising (Abbas et al., 2003).

2.7 Heat transfer during pyrolysis

The start of pyrolysis in different parts of the fuel particle is dependent on the local temperatures throughout the particle. Direct particle temperature measurement is rarely possible and the temperature of a particle is normally calculated by means of heat transfer equations.

The influence of heat transfer on pyrolysis is normally removed by presenting the measured rate data at the particle temperature. As stated by Solomon et al. (1992), inaccuracies in determining particle temperature (either by measurement or calculation) lead to inaccuracies in presented rate data.

2.7.1 Heat conduction in particle

Thermal conductivity of a particle is an indicator of its ability to internally conduct heat. The heat conduction in a particle is controlled by the thermal conductivity, which is dependent both on the density of the particle and its temperature.

According to Solomon et al. (1992), the rise in the thermal conductivity of organic fuels with increasing temperature has been attributed to:

- Radiant heat transfer across pores and cracks.
- Changes in the conductivity of the fuel due to devolatilization.
- Changes in intrinsic conductivity with temperature.

During devolatilization, the flow of escaping volatiles slows down the internal heat transfer. Additionally, if a particle is wet, the evaporation of water significantly slows down heat conduction.

2.7.2 Radiant heat transfer

Radiant heat transfer takes place between a particle and the reactor walls. If the surrounding gas consists of radiative gases, such as water vapour and carbon dioxide, the radiant heat transfer between gas components and particle must be taken into account. In heat transfer calculations, the fuel particle is normally assumed to be a grey particle with an emissivity value of 0.8-0.9 (Solomon et al., 1993a).

2.7.3 Convective heat transfer

According to Saastamoinen (2002), the convective heat transfer coefficient *h* for spherical particles in forced convection can be calculated using the Ranz-Marshall correlation:

$$Nu = \frac{hd_p}{\lambda_g} = 2 + 0.6\,\mathrm{Pr}^{1/3}\,\mathrm{Re}^{1/2} \qquad (2.23)$$

During flash pyrolysis, the flow of released volatiles (i.e. Stefan flow) decreases the heat transfer to the particle. The heat transfer coefficient can be reduced to less than 10% of its original value in conditions of strong transpirational cooling.

The effect of transpirational cooling can be determined for a hypothetical spherical particle in a stagnant gas or, when Reynolds number is very small, from film theory using the following correction factor (Solomon et al., 1992):

$$\theta = \frac{h}{h_0} = \frac{B}{e^B - 1} \tag{2.24}$$

where h_0 is the convective heat transfer coefficient calculated in the absence of cooling and dimensionless transpiration number B is related to the total gas production from a particle by the expression (Saastamoinen, 1984):

$$B = \frac{c_{vol}}{A_p h_0}\left(\frac{dm_p}{dt}\right) \tag{2.25}$$

Here A_p is the surface area of the particle.

However, the assumption of a stagnant film on the surface of a particle usually does not hold with high Reynolds numbers. The following correlation can be used for Reynolds numbers up to 400 (Solomon et al., 1992):

$$\theta = \frac{h}{h_0} = \exp(-0.6B) \tag{2.26}$$

2.8 Particle motion

The relative velocity difference between the gas and the particle (i.e. the slip velocity) has an effect on the convective heat transfer. If the relative velocity difference is great, convective heat transfer between the particle surface and gas becomes more effective.

Particle motion in an external force field can be written as (Flagan and Seinfeld, 1988):

$$m_p \frac{d\vec{v}_p}{dt} = \frac{1}{2} \widetilde{A}_p C_D \rho_g \left(\vec{v}_g - \vec{v}_p\right)\left|\vec{v}_g - \vec{v}_p\right| + m_p \vec{g} \tag{2.27}$$

in which m_p is the mass of the particle, $\widetilde{A}$ is the projected area of the body normal to the flow, C_D is the drag coefficient of the particle, ρ_g is the density of the gas, $\vec{v}_g$ is the velocity of the gas, $\vec{v}_p$ is the velocity of the particle and $\vec{g}$ is the acceleration of the gravity.

Taking the effect of buoyancy into consideration and assuming the particle trajectory to be non-rotational, Equation 2.27 can be written as:

$$\frac{d\vec{v}_p}{dt} = \frac{3}{4} \frac{C_D \rho_g}{d_p \rho_p} \left(\vec{v}_g - \vec{v}_p\right)\left|\vec{v}_g - \vec{v}_p\right| + \frac{\rho_p - \rho_g}{\rho_p} \vec{g} \tag{2.28}$$

The characteristic time τ, which describes the time needed for a particle to adjust to a new condition of forces, can be written for spherical particles as:

$$\tau = \frac{4 \rho_p d_p^2}{3 C_D \mu_g \mathrm{Re}_p} \tag{2.29}$$

Here μ_g is the dynamic viscosity of the gas.

Substituting τ into Equation 2.28 and integrating, the transient velocity of the particle can be written as:

$$\vec{v}_p = \vec{v}_g - \left(\vec{v}_g - \vec{v}_p^{\,0}\right) e^{-\Delta t / \tau} + \tau \frac{\rho_p - \rho_g}{\rho_p} \vec{g} \left(1 - e^{-\Delta t / \tau}\right) \tag{2.30}$$

The correlations for the drag coefficient of spherical particles are given by Hinds (Hinds, 1999):

$$C_D = \frac{24}{\mathrm{Re}_p} \qquad \mathrm{Re_p}<0.1 \qquad (2.31)$$

$$C_D = \frac{24}{\mathrm{Re}_p}\left(1 + \frac{3}{16}\mathrm{Re}_p + \frac{9}{160}\mathrm{Re}_p^2 \ln 2\,\mathrm{Re}_p\right) \qquad 0.1<\mathrm{Re_p}<2 \qquad (2.32)$$

$$C_D = \frac{24}{\mathrm{Re}_p}\left(1 + 0.15\,\mathrm{Re}_p^{0.687}\right) \qquad 2<\mathrm{Re_p}<500 \qquad (2.33)$$

$$C_D = 0.44 \qquad \mathrm{Re_p}>500 \qquad (2.34)$$

The corrected drag coefficient C_D^*, which takes Stefan flow into account, is given by Phuoc and Durbetaki (1987):

$$C_D^* = C_D \exp(-B) \qquad (2.35)$$

2.9 Properties of fuel

When a particle is heated, its chemical, structural and physical properties change with the temperature. Depending on the particle size, these changes might have a significant effect on the rate of pyrolysis and temperature history. If the test environment is such that particle temperature cannot be directly measured or reliably estimated, the particle temperature is normally calculated from the energy balance of the particle. Therefore, in order to accurately determine the kinetic parameters from test results, the temperature dependency of the fuel properties must be taken into account. Although the literature offers only limited information regarding the thermal properties of peat and biomass at high temperatures, it is assumed that these can be reliably approximated with the models presented in the following.

2.9.1 True density and porosity

Merrick has proposed correlations for the true density and porosity of coal and char based on the concept of additive contributions for the elements present (Merrick 1993b). The bulk density of the particle ρ_p is based on the measurement done according to the outer surface of the particle, whereas the true density ρ_t of a dry ash-free particle can be calculated according to Merrick (1993b) as:

$$\frac{1}{\rho_t} = \sum_{i=1}^{5} \alpha_i \gamma_i / M_i \tag{2.36}$$

where γ_i are the mass fractions of carbon, hydrogen, oxygen, nitrogen and sulphur on a dry ash-free basis, M_i are the atomic weights of the elements (12, 1, 16, 14 and 32) and α_i are the coefficients of the elements given in Table 2.2.

Table 2.2. Coefficients for Equation 2.36 (Merrick, 1993b).

	C	*H*	*O*	*N*	*S*
α_i ($m^3 kmol^{-1}$)	0.00530	0.00577	0.00346	0.00669	0.00384

Furthermore, the effects of moisture and ash on the true density can be taken into account as (Merrick, 1993b):

$$\frac{1}{\rho_T} = \frac{\gamma_{daf}}{\rho_t} + \frac{\gamma_{ash}}{\rho_{ash}} + \frac{\gamma_w}{\rho_w} \tag{2.37}$$

where ρ_{ash} and ρ_w are the densities of the ash and water and γ_{daf}, γ_{ash} and γ_w are the mass fractions of the dry ash-free fuel, ash and water, respectively.

Peat and biomass fuels usually have a high volatile matter content and during pyrolysis their density decreases significantly. Using a constant diameter model, the density of a particle ρ during pyrolysis can be calculated as (Raiko, 1986):

$$\rho = \rho_0 (1 - V) \tag{2.38}$$

where ρ_0 is the initial density of the particle.

The porosity of the particle affects the rates of heat and mass transfer, and therefore has a significant effect on the rate of pyrolysis. At high heating rates the evolution of volatiles is fast, which results in spherical cavities in char. According to Merrick, the porosity of char ε can be calculated as (Merrick, 1993b):

$$\varepsilon = 1 - \frac{\rho_p}{\rho_T} \tag{2.39}$$

The correlation for the increase in porosity of the particle during pyrolysis is given by Bliek et al. as (1985):

$$\varepsilon_p = \varepsilon_0 + (\varepsilon_\infty - \varepsilon_0)\left(\frac{\rho_0 - \rho_p}{\rho_0 - \rho_\infty}\right) \tag{2.40}$$

In Equation 2.40, ε_0 is the porosity of the particle before pyrolysis and ε_∞ is the porosity of the particle after pyrolysis.

2.9.2 Specific heat

Proper calculations for various pyrolysis, combustion and conversion processes require the specific heat of material to be known to construct an accurate energy balance. The Merrick model for specific heat has been found to be in reasonable agreement with recent measurements of a large number of coals. Merrick uses the Einstein form of quantum theory to describe the variation in specific heat with temperature and determines the effect of composition by assuming that all atoms in solid matter oscillate independently in three dimensions, with a common characteristic frequency. In the model, the mean atomic vibration is described by two temperatures T_{E1} and T_{E2}, called the Einstein temperatures (Merrick, 1993a).

The average molar weight of a fuel M_{ave} can be calculated as (Merrick, 1993a):

$$\frac{1}{M_{ave}} = \sum_{i=1}^{5} \gamma_i / M_i \tag{2.41}$$

In the Merrick model, the specific heat is calculated using two Einstein temperatures as follows (Merrick, 1993a):

$$c_{p,daf} = \frac{R_u}{M_{ave}}\left[\left(\frac{T_{E1}}{T}\right)^2 \frac{e^{T_{E1}/T}}{\left(e^{T_{E1}/T}-1\right)^2} + 2\left(\frac{T_{E2}}{T}\right)^2 \frac{e^{T_{E2}/T}}{\left(e^{T_{E2}/T}-1\right)^2}\right] \tag{2.42}$$

With proper selection of Einstein temperatures (e.g. T_{E1}=380K and T_{E2}=1800 K) the model has shown good accuracy in predicting specific heats (Solomon et al., 1992) (Hall et al., 1993). The effect of ash and water on specific heat is taken into account as (Merrick, 1993a):

$$c_p = \gamma_{daf} c_{p,daf} + \gamma_{ash} c_{ash} + \gamma_w c_w \tag{2.43}$$

For the ash in the fuel and char, the following correlation can be used:

$$c_{ash} = 754 + 0.586T \tag{2.44}$$

Some correlations for biomass fuels can be found in the literature (Saastamoinen, 1984) (Koufopanos et al., 1989) (Gurgel, 1994) (Gronli, 1996). However, most of them are not temperature-dependent or are otherwise very simplistic.

2.9.3 Thermal conductivity

The heat conduction in wet, porous solid matter is due to the following mechanisms:

- Conduction in solid matter.
- Conduction in gas phase.
- Conduction due to radiation.
- Conduction in liquid phase.
- Conduction due to convection.

In porous materials like peat and biomass, the gas phase constitutes a major part of a particle's volume. In such cases the thermal conductivity of the gas phase is a significant part of the total heat conductivity. In the pyrolysis and gasification of small peat and biomass particles, due to the relatively small size of pores the radiant heat transfer is usually not significant. The main mechanisms of conduction are illustrated in Figure 2.2.

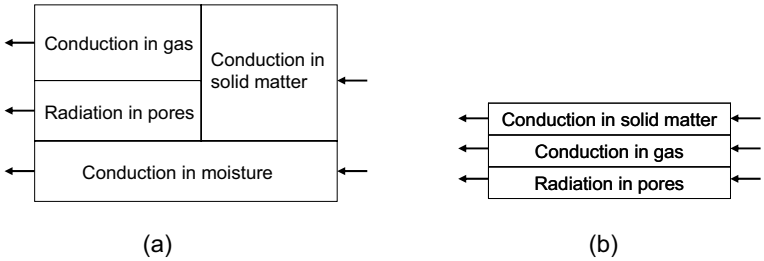

Figure 2.2. Conduction mechanisms: a) conduction model of un-reacted fuel and b) conduction model for char.

In the Merrick model, the effects of the temperature and the composition of the fuel on thermal conductivity are taken into account. According to Merrick, the conduction in solid fuel and char can be calculated as (Merrick, 1993c):

$$\lambda_S = \left(\frac{\rho_t}{4511} \right)^{3.5} T^{0.5} \tag{2.45}$$

The effect of radiant heat transfer in pores can be calculated using the correlation (Merrick, 1993c):

$$\lambda_{rad} = 4\sigma T^3 d_{pore} \tag{2.46}$$

where σ is the Stefan-Boltzmann constant and d_{pore} is the diameter of the pore.

During pyrolysis, the pores of char contain several different gases. However, the thermal conductivity of gaseous products in the fuel and in the char can be approximated with reasonable accuracy using the following correlation for water vapour (Merrick, 1993c):

$$\lambda_g^{act,c} = 7.45 * 10^{-5} T \tag{2.47}$$

The heat conductivity of solid matter is much greater than that of a gas. Therefore, the effective porosity ε_{eff} is calculated as (Merrick, 1993c):

$$\varepsilon_{eff} = 1 - (1 - \varepsilon)^{1/3} \tag{2.48}$$

For the un-reacted fuel, the effective thermal conductivity can be written as (Merrick, 1993c):

$$\lambda_{eff}^{act} = \gamma_w \lambda_w + \frac{1 - \gamma_w}{\varepsilon_{eff} / (\lambda_g^{act} + \lambda_{rad}) + (1 - \varepsilon_{eff}) / \lambda_S} \tag{2.49}$$

After pyrolysis, a fuel particle is porous, and both the solid and gas phases can be considered to be continuous. As presented in the model in Figure 2.2, the thermal conductivity of the char can be calculated as (Merrick, 1993c):

$$\lambda_{eff}^{c} = (1 - \varepsilon)\lambda_S + \varepsilon \lambda_g^c + \varepsilon \lambda_{rad} \tag{2.50}$$

2.9.4 Reaction enthalpy of pyrolysis reactions

Reaction enthalpies change with change in temperature and fuel composition during pyrolysis, but in most calculation models a constant value is used. According to Aho et al. (1989), these energies are difficult to measure because of the inaccuracies associated with low energy emittance and the release of pyrolysis products. Older publications suggest that the heat of pyrolysis is exothermic, but present publications indicate that the total heat of pyrolysis of wood, cellulose and lignin is in fact endothermic at normal pressure.

Aho et al. (1989) measured the reaction enthalpies of peat and reported that the heat of pyrolysis varied between 120 and 250 kJ/kg.

2.10 Modeling of peat and biomass pyrolysis

In modeling the pyrolysis of small or porous particles, the mass transfer can be assumed to be significantly faster than the heat transfer. In the following, the general models for pyrolysis modeling as well as a few special cases are presented.

2.10.1 General model

For the pyrolysis of the peat and biomass particles, the general equation of energy is presented by Saastamoinen (2002):

$$\rho_p c_p \frac{\partial T}{\partial t} = \frac{1}{r^2}\frac{\partial}{\partial r}\left(\lambda_p r^2 \frac{\partial T}{\partial r}\right) - c_{vol}\dot{m}''_{vol}\frac{\partial T}{\partial r} + q_{pyr}\frac{\partial \rho_p}{\partial t} \tag{2.51}$$

where $\dot{m}''_{vol}$ is the mass flux of the volatile compounds and q_{pyr} is the reaction enthalpy of the pyrolysis reactions. The general model takes both internal and external heat transfer and chemical kinetics into account, in which case the temperature distribution in a particle changes during pyrolysis. The left part of the equation describes the energy conservation in the particle, whereas on the right side the first term describes the thermal heat conduction, the second term describes the convective heat transfer between pyrolysis gases and solid matter and the last part describes the generation or consumption of thermal energy.

The mass flux of the volatile compounds $\dot{m}''_{vol}$ is given as (Raiko, 1986):

$$\dot{m}''_{vol} = \frac{1}{r^2}\int_0^r r^2\left(-\frac{\partial \rho_p}{\partial t}\right)dr \tag{2.52}$$

The kinetics of the pyrolysis can be modeled using the different kinetic models presented in Section 2.6. For example, the one-reaction model can be used as:

$$\frac{\partial \rho_p}{\partial t} = -Ae^{\left(\frac{-E}{R_u T}\right)}\left(\rho_p - \rho_\infty\right) \tag{2.53}$$

and the two-competing-reactions model can be used as:

$$\frac{d\rho_{act}}{dt} = -(k_1 + k_2)\rho_{act} \tag{2.54}$$

$$\frac{d\rho_{vol}}{dt} = (y_1 k_1 + y_2 k_2)\rho_{act} \tag{2.55}$$

$$\frac{d\rho_c}{dt} = \left[(1 - y_1)k_1 + (1 - y_2)k_2\right]\rho_{act} \tag{2.56}$$

The initial and boundary conditions for the equations are:

$$T = T_0,\ \rho_p = \rho_0, \rho_{act} = \rho_0 \qquad 0< r < r_0,\ t = 0 \tag{2.57}$$

$$\rho_{act} = 0 \qquad 0< r < r_0,\ t =\infty \tag{2.58}$$

$$\left.\frac{\partial T}{\partial r}\right|_{r=0} = 0 \tag{2.59}$$

$$\lambda_p \left.\frac{\partial T}{\partial r}\right|_{r=r_0} = \theta\, h_o\left(T_g - T_s\right) + \varepsilon\sigma\left(T_w^4 - T_s^4\right) \qquad t > 0 \tag{2.60}$$

Combining radiant and convective heat transfer and taking Stefan flow into account, the effective heat transfer coefficient can be written as:

$$h_{eff} = \frac{\dot{C}_s''}{\exp(\dot{C}_s'' d_p / Nu_0 \lambda_g) - 1} + \varepsilon\sigma \frac{T_w^4 - T_s^4}{T_g - T_s} \tag{2.61}$$

where $\dot{C}_s''$ is the heat capacity flux of volatiles from particle surface and Nu_0 is the Nusselt number calculated without Stefan flow.

As a result, the boundary condition, i.e. Equation 2.60, can be written as:

$$\lambda_p \left.\frac{\partial T}{\partial r}\right|_{r=r_0} = h_{eff}\left(T_g - T_s\right) \tag{2.62}$$

2.10.2 Pyrolysis controlled by chemical kinetics and external heat transfer

If the internal heat conduction is very fast, a particle is practically at uniform temperature and pyrolysis takes place equally throughout the particle. In that case the energy equation and boundary condition 2.60 are simplified, giving (Fletcher et al., 1993):

$$V_p \rho_p c_p \frac{\partial T}{\partial t} = \theta h_o A_p (T_g - T) + \varepsilon \sigma A_p (T_w^4 - T^4) + V_p q_{pyr} \frac{\partial \rho_p}{\partial t}$$

$$= h_{eff} A_p (T_g - T) + V_p q_{pyr} \frac{\partial \rho_p}{\partial t} \qquad (2.63)$$

Here V_p is the volume of the particle.

2.10.3 Pyrolysis controlled by chemical kinetics

If the external and internal heat transfer processes are faster than the chemical reactions, the particle can be assumed to be at uniform temperature with the surrounding gas. In that case, the particle size does not have an effect on the rate of pyrolysis and the reactions take place isothermally at the temperature $T = T_g$.

Then the Equation 2.53 can be integrated, giving (Pyle and Zaror, 1984):

$$\frac{\rho_p - \rho_c}{\rho_0 - \rho_c} = \exp\left[- At \exp\left(\frac{-E}{R_u T_g} \right) \right] \qquad (2.64)$$

Equation 2.64 is suitable for conditions where only the chemical kinetics are controlling the rate of pyrolysis and where pyrolysis can be described using a single first-order model.

CHAPTER 3

Common laboratory-scale analysis methods

Laboratory-scale measuring equipment and methods are suitable for characterization of fuels, determining the principles of the physics and chemistry of combustion, predicting problems of full-scale combustion devices and seeking solutions for these problems. More recently, understanding pollutant formation, ash sintering and corrosion have become increasingly important. The effects of fuel properties and operating conditions on the formation of NO_x and SO_2 as well as problems of mineral/deposit and fuel characterization have been studied extensively in recent years.

According to Aho (2002), with laboratory-scale equipment, the test conditions are more alterable and easier to handle than with bench, pilot or full-scale devices. Well-designed laboratory-scale measuring equipment has good controllability and provides direct and repeatable experimental initial data for the mathematical modeling of full-scale combustion devices. Importantly, laboratory-scale equipment is usually significantly cheaper to build and operate than bench, pilot or full-scale devices (Aho, 2002).

This chapter presents some of the most common laboratory-scale analysis methods. In addition to those methods discussed later in this chapter, some other methods, such as pyrolysis mass spectrometry, pyroprobe and small-scale fluidized beds are noted.

A summary of some typical operational conditions is presented in Table 3.1 (Heikkinen, 2005).

Table 3.1. Some typical operational conditions presented by Heikkinen (2005).

	Particle size (mm)	*Heating rate (K/s)*	*Temperature (°C)*	*Residence time (s)*
Pulverized coal boiler	< 0.1	$>10^5$	1300-1700	≈ 1
Thermogravimetric analysis	≤ 2	<1.67	1500	≈ 3600
Heated wire mesh	≤ 2	10^3	800-1400	1-5
PF reactor	< 0.5	$>10^4$	<1500	2-3

3.1 Standardized methods

Standardized methods are used to determine the proximate analysis of fuel, which gives e.g. the proportion of volatile matter that is contained in the fuel. Volatiles are released during pyrolysis, i.e. when a fuel sample is heated up to an adequate temperature in inert conditions. The absence of oxygen ensures that no combustion takes place and thus the weight loss during heating represents only the volatile matter contained in the sample.

The procedure for determining the volatile matter content of coal can be found e.g. in standard ISO 562 (Hard coal and coke – Determination of volatile matter). A 1g–sized sample of fuel is placed in a lidded crucible, which is put into a pre-heated furnace. The sample is kept at 900±10°C for seven minutes. The lid prevents oxygen from reaching the sample, and the oxygen that is initially in the crucible is consumed as the evolving volatiles burn inside the crucible. By weighing the sample before and after the experiment, the amount of volatile matter is obtained. The result is usually given as the percent by weight of the original sample, either on a dry or wet basis. Along with ISO 562, DIN 51720 (Bestimmung des Gehaltes an Flüchtigen Bestandteilen) is widely used in measuring the volatile content. The procedures regarding sample size, temperature, heating rate and residence time are identical to those described in ISO 562. At the moment, no standard procedure exists for the determination of volatile matter in biomass.

3.2 Heated wire mesh (HWM)

Heated wire mesh (also called heated grid or screen heater) is mainly used to study pyrolysis and gasification of solid fuels (Heikkinen, 2005). HWM provides a high temperature and high heating rate test in conditions nearer those of FB combustion than current standardized proximate analysis methods. However, it is a complex technique and has heat transfer limitations. Consequently, it has uncertain particle temperatures at high heating rates (Heikkinen, 2005).

Even though most screen heaters are in-house built, the reactor typically has a cylindrical housing in which a fine metal grid (mesh) is placed between electrodes (Heikkinen, 2005). A thin layer of fuel particles is placed on the mesh and when voltage from an external power supply is increased between the electrodes, a current flows through the mesh and heats it (Heikkinen, 2005). By proper adjustment of the current to the mesh, the heating rate as well as the peak temperature and its holding time can be independently controlled (Carpenter and Skorupska, 1993). The temperature history of the fuel particles is usually assumed to be the same as for a thermocouple bead, which is either attached to the wire mesh or placed within its folds (Solomon et al., 1993b) (Aho, 2002). The mesh is sealed within a cell that may contain the specified gas atmosphere (e.g. nitrogen and/or helium). In the tests, pyrolysis weight loss is obtained by weighing the sample prior to pyrolysis and afterwards. The reactor can be operated in pressurized conditions or in a vacuum, depending on the application (Aho, 2002).

The advantages of HWM include linear and reproducible heating rate, which is important particularly in kinetic studies. Also, the time of pyrolysis can be precisely controlled and a good material balance can be achieved. Further, since the volatiles enter a cold environment upon leaving the mesh, secondary reactions are minimized, although not totally eliminated. HWM as a method is inexpensive, simple and fast to use, and the composition of product gas is measurable (Carpenter and Skorupska, 1993) (Solomon et al., 1993b) (Aho, 2002).

However, heat transfer between the sample holder and the sample itself may not be good enough to prevent significant temperature gradients inside the sample. Thus, determination of the real particle temperature is uncertain during the heat-up, which limits the use of the method as a standard pyrolysis test. The maximum heat rate and the peak temperature obtainable in the HWM are both lower than the corresponding values reached in commercial PF boilers, but they fit quite well the values of FB boilers. Furthermore, as the sample particles are not free to move as they do in commercial boilers, the heated mesh apparatus does not simulate conditions in real FB or PF boilers. Although secondary reactions are limited, some of the volatiles may be altered by catalytic cracking on the hot mesh or by secondary reactions on the walls of the reactor. Also, the mesh itself can oxidize particles, thus affecting the accuracy of weight loss measurements (Carpenter and Skorupska, 1993) (Aho, 2002).

3.3 Thermogravimetric analysis (TGA)

Thermogravimetry is one of the oldest thermal analytical procedures used in research laboratories. A common thermogravimetric analyser (also called a thermobalance) consists of an accurate microbalance and a furnace and control system (Heikkinen, 2005). In a thermobalance, fuel sample is heated in a well-controlled atmosphere. As a result, the mass loss rate and the mass of the sample can be derived as a function of time. The mass of the sample may be observed as a function of the temperature or the sample may be kept at a constant temperature. The pressure can range from high vacuum to elevated and high pressure.

The greatest disadvantage of this method is generally slow heating rate, which is of the order of some tens of degrees per minute, when compared to large-scale combustors. This affects strongly the amount of volatiles released and thus diminishes the reliability of the measured values. Another great disadvantage of TGA is the difficulty in determining the exact sample temperature (Carpenter and Skorupska, 1993) (Aho, 2002) (Heikkinen, 2005).

On the other hand, TGA is well suited for pyrolysis, combustion and gasification studies of single, large fuel particles. Also, TGA is a good method for comparing the reactivity of different fuels. Additionally, TGA has good mass balance, time and temperature control and minimum secondary reactions, and it permits the handling of all fuels and all sizes of fuels that are studied. TGA can be summed up as a versatile, reproducible, precise, objective, fast and relatively cheap method that is commercially available (Carpenter and Skorupska, 1993) (Aho, 2002) (Heikkinen, 2005). However, TGA does not actually simulate PF or FB conditions, and kinetic parameters derived from pyrolysis test results are only useable for slow pyrolysis.

3.4 Drop tube reactor (DTR) and entrained flow reactor (EFR)

DTR/EFR reactors provide high volatile yields at heating rates close to those occurring in industrial combustors. Combustion kinetic data derived from these reactors can be used for large-scale combustion modeling, to examine mineral matter transformation and ash deposition and to study NO_x formation mechanisms. Although these methods simulate best the conditions in a typical combustion furnace, the heating rates are neither linear nor measurable, making reproducibility of a test sometimes difficult. Also, most of these kinds of reactors operate in laminar flow regime. Therefore, the results cannot be directly applied to particles in a turbulent state, which is the case in large-scale combustion units.

The relationship between the flow rate of the gas stream and the terminal velocity of the free-falling fuel particles determines whether the particles are dropped or entrained through the reactor tube. If the terminal velocity of a particle is less than the gas velocity, the particle is entrained.

In the literature, numerous studies based on these types of reactors can be found for coal. Recently, studies for biomass have been presented as well, for example by Brown et al. (2001) and by Biagini et al. (2005).

3.4.1 Drop tube reactor (DTR)

Drop tube reactors are designed to study reactions of small fuel particles (typically < 200 μm) in heating rate conditions similar to those in FB and PF boilers and at high temperatures up to 1800ºC. In this type of reactor, a small and continuous mass flow of fuel particles is fed along an inert carrier gas flow to a cylindrical reactor tube that is surrounded by several controllable electric resistance units to produce and maintain isothermal conditions along the length of the reaction zone. The feeding of a fuel is always carried out downwards from the top (Carpenter and Skorupska, 1993) (Aho, 2002).

Furthermore, the reactant gas, with a specific adjustable composition, is directed to the tube distinctly in the laminar regime (Re < 2200) with the aim of having the fuel flow form a flat band of single particles travelling along the centreline of the reaction tube. The feeding rate of the particles is set so small that it has no effect on the temperature and gas composition in the reaction zone of the tube. Next, the product particles that remain after the sample has travelled through the reaction zone are collected by a water-cooled probe or by using e.g. a liquid nitrogen quench. The quenched solid products are usually separated from the gases via a cyclone as the products are drawn through the collection system by a pump. Because water and tars might condense in the cyclone and contaminate the solid products, the cyclone must be kept above 200ºC to prevent such problems. The weight loss has typically been determined by the ash tracer method or by simply comparing the total mass of fuel fed with the char collected. The residence time of the sample within the reaction zone of the tube is mainly controlled by the positions of the sample injector and the product collector along the axis of the tube and by gas velocity (Aho, 2002).

The DTR can provide high heating rates and temperatures close to FB and PF conditions. Mass balances and residence times are moderately well controlled and known (these issues are also covered in Chapter 4). Also, the reactor is able to handle all types of fuels. One of the disadvantages of the DTR method is that usually heating rates are not linear. Moreover, the volatile products remain hot

during the experiments and thus might undergo secondary reactions. However, the major disadvantage is that fuel particle temperature histories are difficult to determine. The accurate details of the mixing of the fuel and carrier gas with the reactant gas, which are not usually known, are very important for the precise prediction of temperatures. That is, a laminar flow profile can produce poor particle-gas mixing. In summary, simplifications and standardisation of equipment are essential before DTRs can become a routine test (Carpenter and Skorupska, 1993) (Aho, 2002).

3.4.2 Entrained flow reactor (EFR)

In entrained flow reactors, fuel is directed to the entire cross-section of the cylindrical reaction tube. The aim is to get the fuel particles to attain the average gas velocity using a sufficiently high gas velocity, but particle collisions with the reactor walls may slow down their velocity. After rapid mixing of the fuel particles and reactant gas, the combined flow is directed to the tube reactor in which the flow profile corresponds to the plug flow. Therefore, the fuel particles are evenly dispersed throughout the entire reactor cross-section. The residence time in the reactor may be varied by moving the electrode positions to vary the distance over which the tube is hot. Also, adjustment of the gas velocity may be used for changing the residence time (Aho, 2002).

In addition to moderately high heating rates, high temperatures and good mass balance, an advantage of the EFR is that both the particle temperature and the residence time can be directly measured based on the known complete mixing of the reactants if turbulence and wall interactions do not disturb the flow profile. Furthermore, the relatively high mass flow of fuel enables investigation of pollutant formation. The disadvantages of the method include the need to use isokinetic sampling, the possibility of secondary reactions and particle fragmentation due to the high velocities used. Furthermore, the EFR cannot handle softening fuels, because they can stick to the tube walls as a result of wall interactions. Also, entrained flow reactors are relatively expensive to build and fuel preparation for tests is time-consuming (Aho, 2002).

CHAPTER 4

Experimental

One of the objectives of this dissertation was to design, build and characterize a high-heating-rate laboratory-scale reactor capable of determining reliably the volatile content and the rate of release of high-volatile-content solid fuels at different residence times. In this chapter, the developed laminar flow reactor is introduced and characterized. Furthermore, different methods for determining the volatile content of solid fuels are compared. Finally, results of pyrolysis tests carried out with the LFRD for the modeling part of the dissertation are presented.

4.1 Experimental apparatus

In the design of the reactor, one of the main goals was to build a simple reactor with the emphasis on making the moderately accurate determination of volatile yield and particle residence time possible. Laminar flow regime was selected in order to keep particles close to the centreline through the length of the reactor, which allows quite accurate determination of particle residence time in the reactor. Additionally, laminar flow regime was also selected in order to avoid unwanted particle-wall interactions.

The major difference between the LFRD and common DTR/EFR systems is that in the LFRD the fuel particles and cold gas are first premixed and then heated together, whereas in the latter systems the fuel particles are normally fed directly into the hot gas. As discussed in Section 3.4.1, the mixing of cold gas containing the fuel particles with hot reactor gases causes problems in determining particle temperature during heating. Although this problem is avoided with the current reactor, one drawback of the solution is the reduced heating rate. However, the results calculated from the modeling show that the LFRD can achieve heating rates greater than 10^3 K/s (see Section 5.5.6).

Another design feature was to keep the diameter of the reactor small, which makes temperature control of the reactor simple and relatively accurate. The importance of uniform wall and gas temperature profiles of the laminar flow reactor is discussed extensively by Brown et al. (2001).

Accurate determination of volatile yield is possible since the total amounts of fuel particles fed and collected are known. As discussed earlier by Solomon et al. (1993a) and by Bharadwaj et al. (2004), the ash tracer method determines mass loss on the assumption that ash and its tracer species are non-reactive and non-volatile during experiments. According to Solomon et al. (1993a), this procedure suffers from obvious drawbacks associated with potentially volatile ash constituents (like K, Na, S or Cl) or otherwise uncollectible ash constituents. Furthermore, Bharadwaj et al. (2004) point out that traditional tracer species commonly used in coal research (Si, Al and Ti) are often not present in sufficient quantity in many biomass fuels. For example, Ca and Mg could be used as tracer species for wood. In the LFRD, the whole gas flow containing fuel particles is directed through a collecting filter and the total weights of fuel particles fed and of char collected are compared. Solomon et al. (1993a) also estimated that by direct comparison of the total char collected with the total fuel fed (or using the ash tracer method) the weight loss can easily be measured with a range of inaccuracy not greater than 10%, which has only a negligible effect on the kinetic rates.

The LFRD is presented in Figure 4.1. It is constructed using a 12.4 mm inner diameter austenitic chromium-nickel steel tube. The reactor can be continuously operated up to a temperature of 1100°C.

A screw feeder (number 1 in Figure 4.1) is situated on the top of the reactor to feed fuel sample into the centreline of the reactor via a small feeding pipe. The fuel chamber of the screw feeder is made of transparent light plastic.

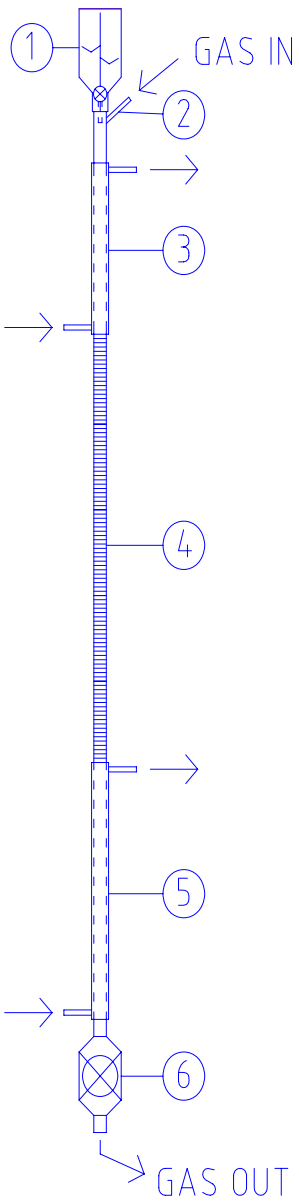

The gas atmosphere in the reactor can be varied, although normally N_2 is used in pyrolysis tests. The gas flow (2) is introduced into the top of the reactor via gas flowmeters. A stabilizing counter-flow heat exchanger (3) is located above the heated tube part. The stabilizing medium can be either air or water, depending on the temperature desired. The purpose of the heat exchanger is to stabilize the inlet temperature and allow the flow containing the particles enough time to fully develop before the heated part.

The reactor part (4) is heated by four independent electric heaters. Five retractable thermocouples are inserted along the length of the reactor. A cooling counter-flow heat exchanger (5) is located below the heated tube part. The cooling medium can be either air or water, depending on the temperature desired. The purpose of the heat exchanger is to cool down the gas and particles as quickly as possible and at the same time keep the temperature high enough to prevent condensation of the tars and other gaseous compounds.

Figure 4.1. Schematic diagram of LFRD.

A microfibre filter in metallic cover (6) is used to capture totally or partly pyrolysed fuel particles. An electric heater is used to keep the cover at high enough temperatures to prevent condensation of tars and other gaseous compounds.

For this research, four different reactors were built. These reactors are completely identical except for the heated reactor parts, which are 0.15, 0.30, 0.50 and 0.70 m long to provide different particle residence times in the reactor.

4.2 Characterization of experimental apparatus

Temperature profiles at the cross-section and along the length of the reactor are important properties of the reactor and these were measured at three different temperature levels and two different gas flows. Also, the effect of the cooling temperature on the volatile yield was tested.

4.2.1 Temperature profiles

The gas temperature profiles inside the reactor were measured at different temperature levels using five retractable thermocouples. The measured gas temperature profiles along the length of the reactor are presented in Figure 4.2.

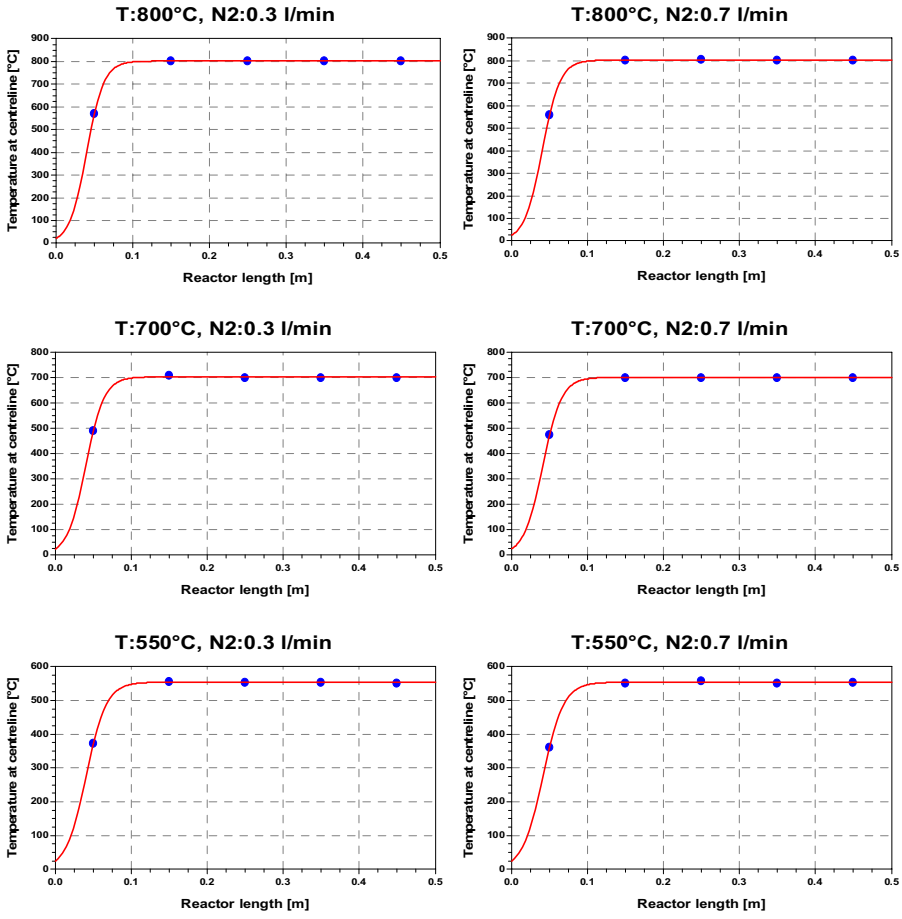

Figure 4.2. Temperature profiles of centreline along length of reactor.

In general, constant gas temperature in the centreline was attained in about the first 10 cm of the reactor length. Also, four independent electric heaters in the heated reactor part were found to give good controllability to the temperature profiles, which were easily repeatable in all test points.

Furthermore, the thermal conditions around the centreline of the reactor can be considered to be practically isothermal. Figure 4.3 illustrates temperatures along the cross-section of the reactor in four different places at the reactor length of 30 cm, namely at the centreline and at +2, + 4 and +6 mm from the centreline at three different temperature levels, i.e. 800°C, 700°C and 550°C.

Figure 4.3 shows that the temperature at +2 mm from the centreline is only 4-9°C higher than the nominal temperature at the centreline, depending on the temperature level. Also, the temperature at the reactor wall (+6 mm away) is only about 8-16°C higher than the nominal temperature. The temperature differences in the cross-sectional direction remained roughly the same in all other measurement points at all temperature levels.

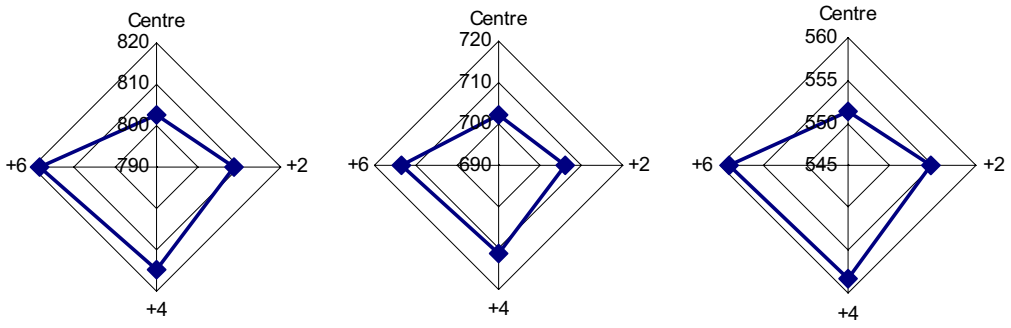

Figure 4.3. Temperature profiles along cross-section.

As reported earlier by Brown et al. (2001), accurate measurement of the wall temperature is critical for calculating the gas temperature in the LFRD. On the basis of the results, the temperature profiles for wall and gas are not expected to be a significant source of error. Radiation correction of temperature measurement was not needed due to the small temperature differences between the gas and wall.

4.2.2 Effect of cooling temperature

Volatiles released from the pyrolysis of the peat and biomass fuels contain a lot of tar, especially at lower temperatures. As mentioned in Section 2.2, tar compounds are gaseous in pyrolysis conditions but condense at room temperature. That was clearly noticed when the temperature of the cooling counter-flow heat exchanger and metallic cover was kept at 20°C instead of 200°C while testing the reactor with peat fuel. The glass microfibre filter inside the metallic cover collected also tar compounds, which caused a major error in the determination of volatile yield. This was easy to notice when the temperature level was high enough in the metallic cover since the glass microfibre filter inside the cover remained completely white throughout the test.

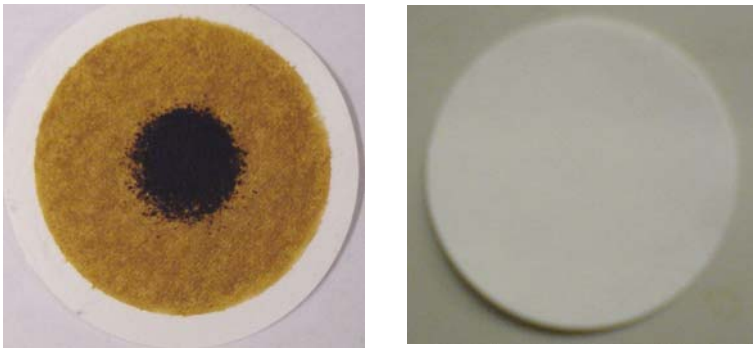

Figure 4.4. Dirty glass microfibre filter on the left, clean filter on the right.

4.3 Optical measurements

In order to calculate the residence time of a particle in the reactor accurately, it was necessary to ensure that the particles stayed close to the centreline along the whole length of the reactor. Therefore, optical measurement techniques were used to determine the cross-sectional positions of the fuel particles at the outlet of the reactor at room temperature with different gas velocities and fuel feeding rates. Also some other key properties of the fuel, such as particle size, shape and velocity were measured at the reactor outlet.

Direct optical measurements using robust image processing methods make it possible to study two-phase flow with particles in air. For such measurements,

peat particles were dropped through the cold reactor, after which individual particles were identified using several series of images. Particle velocities were calculated from consecutive images based on the displacement of a particle and the time difference between the images. The dispersed particle phase was so dilute that particle overlapping did not occur, which made detection of single particles relatively easy and accurate.

A four-frame particle tracking algorithm with a multivariable matching technique is a very efficient and also accurate velocity measurement method when particles are not overlapping in images. All algorithms used have been developed at Tampere University of Technology (TUT). The basic principles of different image processing techniques have been presented by Sonka et al. (1999).

4.3.1 Detection of particles

Only in-focus particles were recognized in order to improve detection accuracy. Particles which were out of focus (in other words in front of or behind the field of depth) were excluded from the particle analysis.

4.3.2 Analysis of particle images

There are several methods for calculating the properties of particles (size, shape, velocity and position) from their two-dimensional projections in an image. However, two-dimensional projections do not completely describe the structure of three-dimensional, irregular-shaped particles. Particles that are shaped e.g. like flakes have completely different projections when seen from different angles.

The diameter of a particle d can be defined as a projected area diameter:

$$d = 2 \cdot \sqrt{\left(\frac{A_{pi}}{\pi} \right)} \tag{4.1}$$

Here A_{pi} is the projected area of the particle image.

The circumference *p* of a particle image is resolved by calculating the number of edge pixels of the particle image. If the edge pixels are defined according to the 4-connectivity rule (north, south, east, west), the result underestimates the perimeter length (i.e. circumference) by 10-40 %. On the other hand, calculation according to the 8-connectivity rule (the eight main compass points) overestimates the perimeter length by 10-20 %. Furthermore, the curvature of the perimeter should be taken into account and the curve length at each edge pixel of the segment should be measured. However, this is time-consuming and therefore the average of the results measured according to the 4- and 8-connectivity rules is defined as the actual circumference of the particle image.

The shape factor *S* is a two-dimensional measure of particle shape. The shape factor is obtained by dividing a square of circumference *p* by its area times 4π. For a sphere, it is defined as:

$$S = \frac{p^2}{4\pi A_{pi}} \hat{=} \frac{(2\pi \cdot r)^2}{4\pi \cdot \pi r^2} = 1 \qquad (4.2)$$

The shape factor increases with increasing irregularity of a particle. If this value is lower than that for a perfect sphere, this is due apparently to errors in determining the perimeter of a particle. In general, the shape factor is very useful in distinguishing between regular and irregular-shaped particles.

4.3.3 Particle velocity measurements

The procedure used for measuring the velocities of single particles in consecutive images is called Particle Tracking Velocimetry (PTV). The velocity of an object in an image can be measured if a sequence of images is recorded using a sufficiently high recording rate. This means that the object must remain in focus and inside the field of view at least in two consecutive images. When the scaling and time delay of images are known, the two-dimensional velocities of moving objects can be estimated. Only the velocity components parallel to the measurement plane can be measured with the single-camera measurement

setup. PTV technique is actually a specific case of Particle Image Velocimetry (PIV), which is described extensively by Raffel et al. (1998). Instead of using statistical analysis in determining the displacement of many tracer particles, as in PIV, in PTV a single object is recognized in consecutive images and displacement is determined using correlation techniques.

The required recording rate was in this case 200 frames per second. As a result, particles moved between the two consecutive frames even more than 200 pixels. The usual displacements in conventional cross-correlation analysis of PIV images are 1-10 pixels. In this case, long displacements made it necessary to use such large interrogation areas as 256x256 or 512x512 pixels. However, this did not disturb correlation in this particular case because there were only a few particles in each image.

4.3.4 Experimental setup

Peat particles ranging widely in size from 70-350 μm were dropped through the cold reactor while using two different nitrogen flows, i.e. 0.3 l/min and 0.7 l/min. The size, shape, velocity and position of the particles were measured. The measurement setup is presented in Figure 4.5.

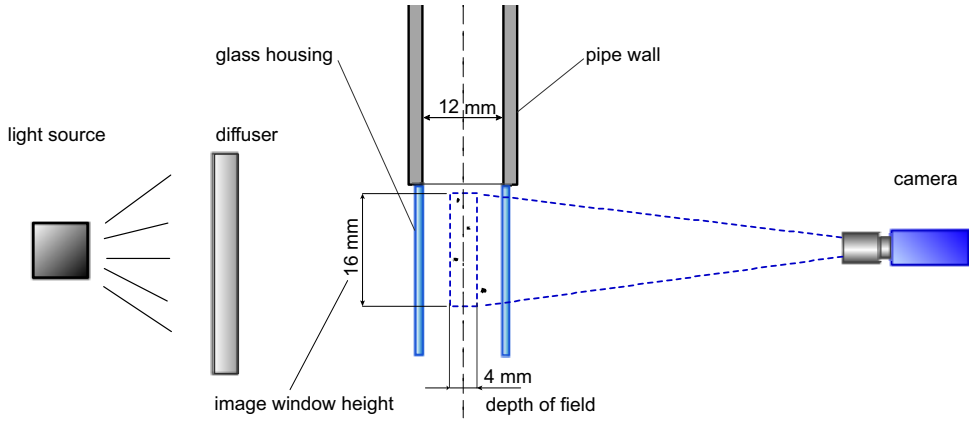

Figure 4.5. Side-view of measurement setup for dropping particles.

Glass pipe housing of reactor diameter was used as a see-through extension to prevent effects of secondary flows in the measurement space. The camera was focused on the reactor centreline with a 4 mm depth of field. The image window was 16 mm and 12 mm in vertical and horizontal directions, respectively. Particle size and gas flow rate combinations were measured at a recording rate of 200 frames per second for 28 seconds, producing 5600 images for each combination. The high-speed camera Imager Pro HS by LaVision with a maximum frame rate of 636 frames per second was used.

In order to produce shadow images of the particles with a very bright and smooth background, a diffuser was used between the floodlight and the image plane. Special care was taken to align the reactor vertically, using a plumb line as a check. The reactor was protected with a multilayer aluminium foil to prevent it from warming due to thermal radiation emitted from the light source. This prevented asymmetric warming of the reactor wall affecting the internal flow profile.

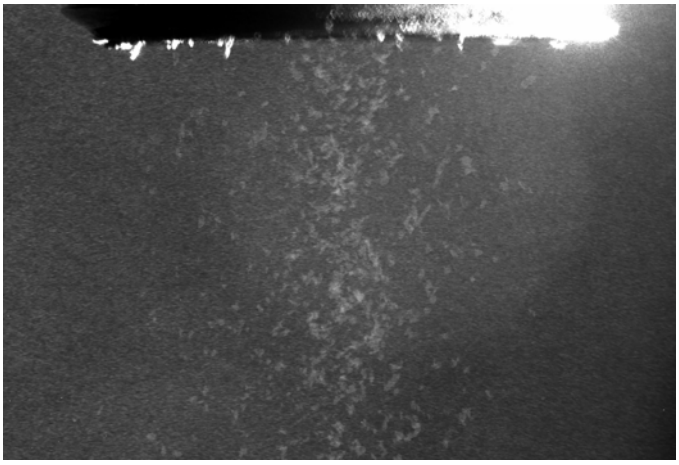

Figure 4.6. Fuel particles dropping out of reactor tube.

4.3.5 Experimental results

Particle shape

In spite of the special care paid to fuel preparation (drying, crushing, sieving and water-sieving), PTV pictures showed the heterogeneous nature of the peat. The particles exhibited variation in both size and shape, as can be seen e.g. in Figure 4.7.

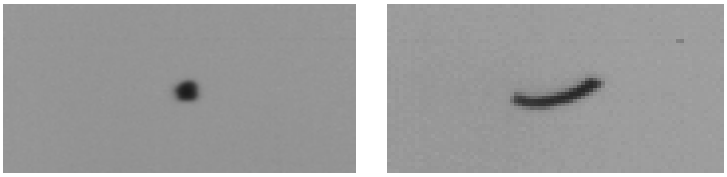

Figure 4.7. Round peat particle on the left and “flake”-like particle on the right.

Similar results have been reported earlier by Bharadwaj et al. (2004). They reported that biomass particles are often irregularly shaped and therefore sieving classifies particles by their smallest dimension.

Particle position

The particle position measurements show that the majority of the particles remain close to the centreline of the reactor. On average, almost 75 % of the particles were closer than 1 mm to the centreline and over 94 % of the particles were located a maximum of 2 mm away from the centreline. The results are presented in Table 4.1 and Figure 4.8.

Table 4.1. Particle positions in reactor outlet.

#	*Description of test point*	*Number of particles*	*Centreline ± 1 mm*	*Centreline ± 2 mm*
1	70-350 μm, N2: 0.3 l/min	131	79.4 %	94.7 %
2	70-350 μm, N2: 0.7 l/min	222	73.2 %	95.0 %
3	70-350 μm, N2: 0.3 l/min	232	70.3 %	93.1 %
4	70-350 μm, N2: 0.7 l/min	141	76.6 %	93.6 %
	Average		74.8 %	94.1 %

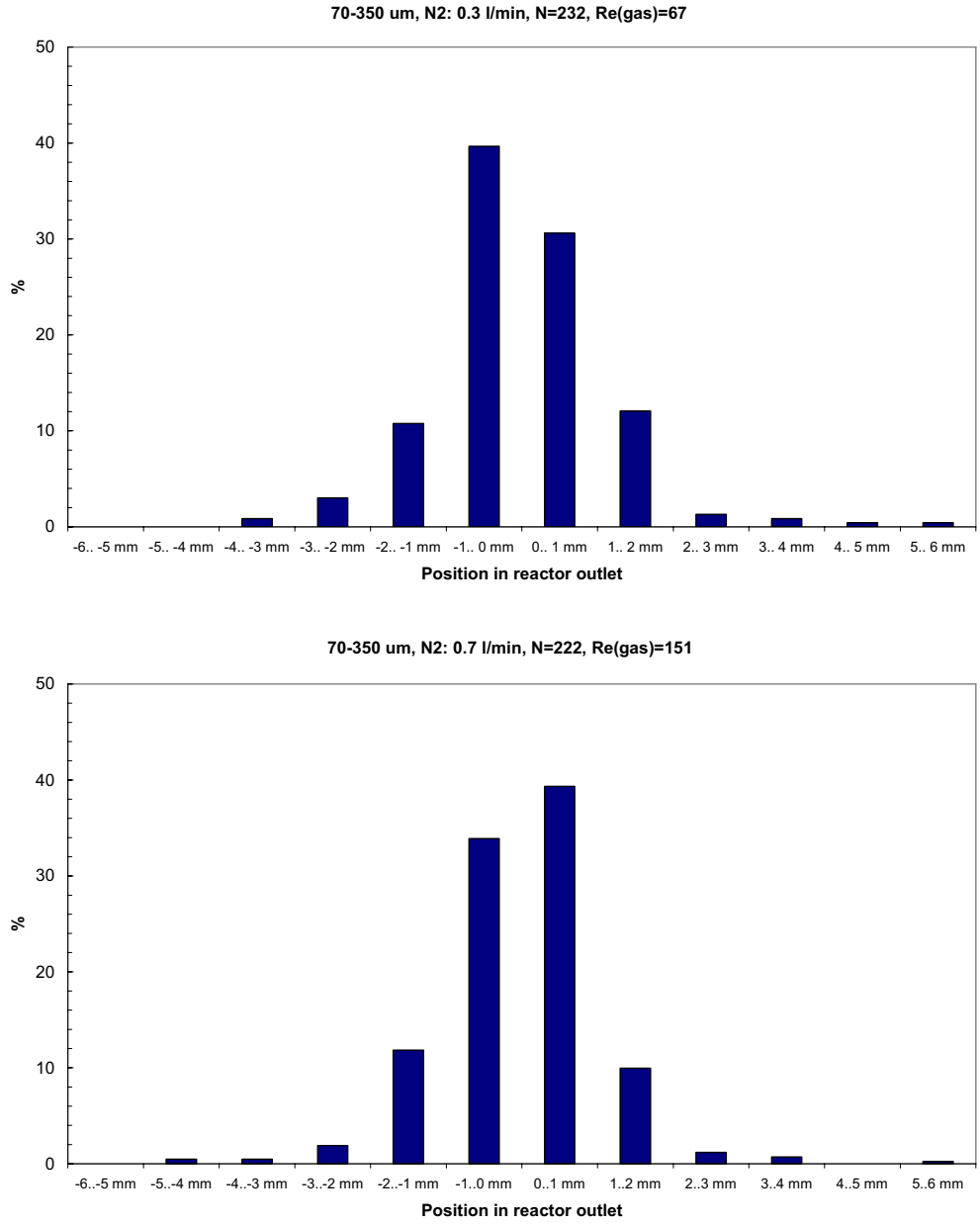

Figure 4.8. Relative density histograms for peat particles classified as a function of radial distance from reactor centreline in selected test points.

In laminar flow conditions, the results indicate that the majority of the particles travel through the reactor in the area where gas velocity is close to the maximum. As presented in Figure 4.9, 75 % of the particles travel through the reactor in the area where the gas velocity is at least 97 % of the maximum gas velocity, whereas 94 % of the particles travel through the reactor in the area where the gas velocity is at least 89 % of the maximum gas velocity.

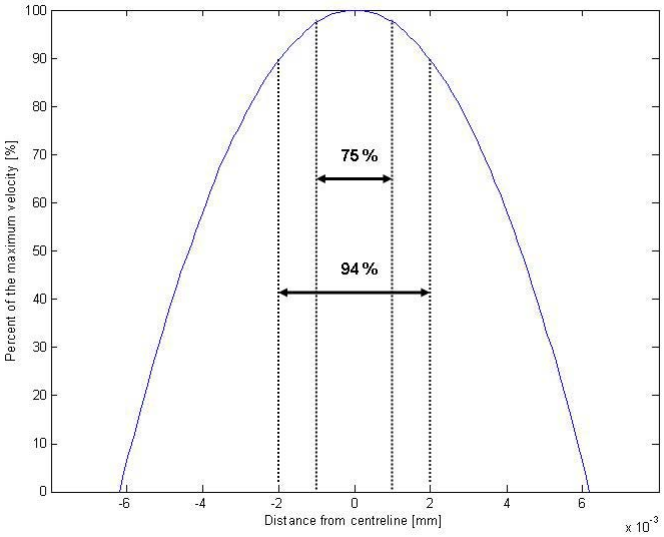

Figure 4.9. Measured particle positions in laminar flow velocity profile.

Particle velocity and drag coefficient

In analysing particle velocity measurement results, it became obvious that terminal velocities of peat particles cannot be explained using drag coefficient correlations for spherical particles presented in Equations 2.31 – 2.34. Even though there was variation in the particle size and velocity, the measured velocities in general were slower than the values predicted from spherical particles. Therefore, for the purposes of pyrolysis modeling, two different particle sizes, 100-125 μm and 180-225 μm, were selected from the results for further analysis. Also, the results presented in Table 4.2 are only for particles with a shape factor between 0.95 and 1.05.

Table 4.2. Measured average particle velocities.

#	*Description of test point*	*Velocity [m/s]*
1	100-125 μm, N2: 0.3 l/min	0.148
2	100-125 μm, N2: 0.7 l/min	0.286
3	180-225 μm, N2: 0.3 l/min	0.386
4	180-225 μm, N2: 0.7 l/min	0.521

For each particle selected for further analysis, the velocity was calculated using Equation 2.30, where the initial estimation of drag coefficient C_D was made according to the correlations given for spherical particles.

The gas velocity $\vec{v}_g$ was calculated from the Newtonian laminar flow velocity profile according to the particle's position in the reactor as follows (Incropera 1996):

$$\vec{v}_g = 2\,(1 - (R / R_o)^2)\,\vec{v}_{g,ave} \tag{4.3}$$

where R is the particle's distance from the reactor centerline, R_0 is the radius of the reactor and $\vec{v}_{g,ave}$ is the average gas velocity.

If the measured and calculated velocities differed, the calculated drag coefficient was multiplied by a correction factor X_{corr} so that the calculated and measured velocities equated. The corrected drag coefficients $C_D^* = C_D \cdot X_{corr}$ as a function of a particle's Reynolds number are presented in Figure 4.10.

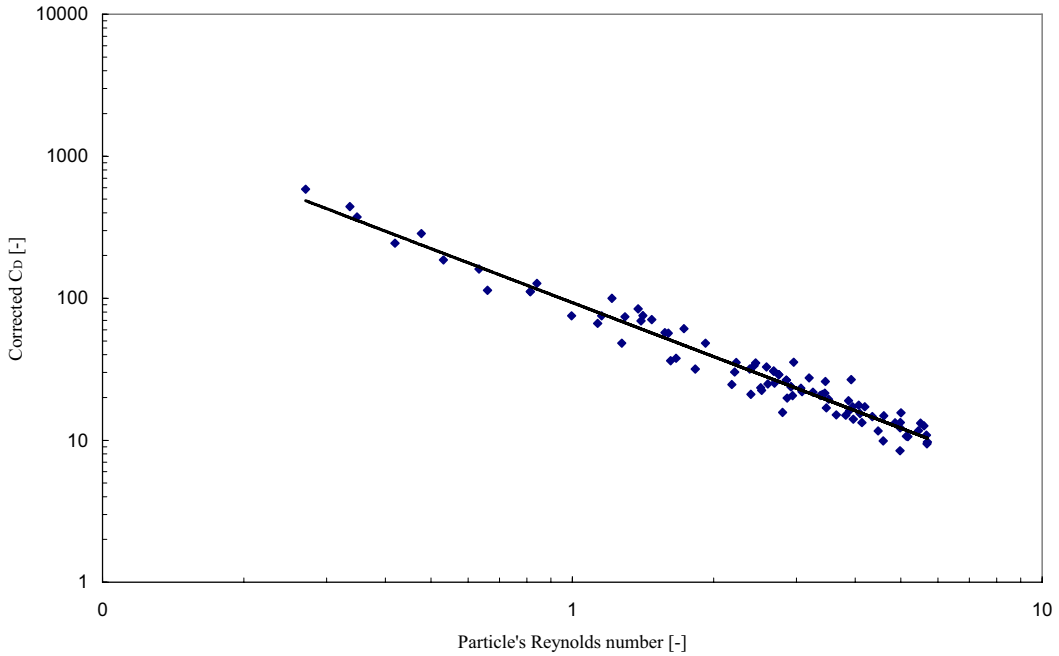

Figure 4.10. Corrected drag coefficient for peat used in experiments.

As Figure 4.10 shows, there are some variations in the corrected drag coefficient values. However, most of the variation can be explained by the heterogeneity of the peat, as noted and discussed in the results for particle shape. Furthermore, studying three-dimensional particles from two-dimensional projections involves some limitations, as discussed in Section 4.3.2. Also, it should be noted that this kind of approach can be assumed to be very case-specific, as the fuel preparation has a significant effect on the size and shape of the fuel particle, especially in the case of heterogeneous fuel like peat.

4.4 Comparison of different analysis methods

Different analysis methods were compared by determining the volatile content of Finnish milled peat fuel (MP) and pine sawdust (PSD) using the LFRD, TGA and standardized laboratory methods with different temperature levels.

4.4.1 Materials

Samples of MP and PSD were dried, crushed and carefully sieved into a particle size fraction of 100-225 μm. The commercial laboratory analyses of the peat and pine sawdust are given in Table 4.3.

Table 4.3. Laboratory analyses of MP and PSD.

Parameter	*Method*	*MP*	*PSD*
Moisture, wt-% (as received)	DIN 51718	31.8	1.2
Volatile matter, wt-% (dry solids)	DIN 51720	67.2	85.2
Ash, wt-% (dry solids) at 550°C	CEN 335	6.1	0.4
Fixed carbon, wt-% (dry solids, calculated)		26.7	14.4
Carbon, wt-% (dry solids)	ASTM D5373	55.1	50.4
Hydrogen, wt-% (dry solids)	ASTM D5373	5.8	6.2
Nitrogen, wt-% (dry solids)	ASTM D5373	1.8	0.1
Sulphur, wt-% (dry solids)	ASTM D4239	0.14	0.01
Oxygen, wt-% (dry solids, calculated)		31.1	42.9

4.4.2 Volatile content measured according to ISO 562

The volatile content of MP was determined using the procedure described in the ISO 562 standard. On the basis of the experiments, the volatile content was determined to be 71.7 % on a dry ash-free basis, being the average of 10 parallel measurements. This result was in good accordance with the result obtained from a commercial laboratory analysis using the DIN 51720 procedure, which gave a value of 71.6 % on a dry ash-free basis for the same peat. Moreover, the procedure proved to be easily reproducible and the variation in the results seemed to derive more from the heterogeneity of the fuel than from the procedure. The margin between the highest and the lowest result of the parallel measurements was 1.2 %.

The temperature level of 550°C turned out to be too low for MP. When samples were heated up using 550°C as final temperature, the average value of 66.8 % on a dry ash-free basis was obtained, which was considerably lower than that reached with the standard method for coal. The commercial laboratory analysis using the DIN 51720 procedure gave a volatile yield of 85.5 % on a dry ash-free basis for the PSD.

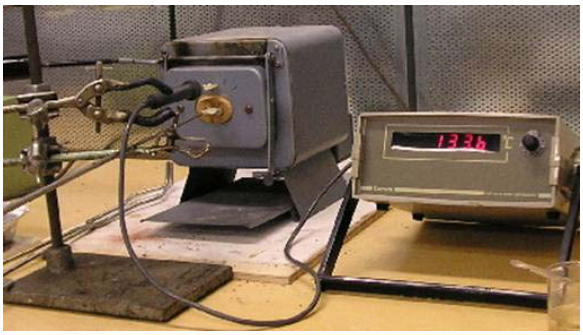

Figure 4.11. ISO 562 test equipment at TUT.

4.4.3 Volatile content measured by TGA

Four thermogravimetric analyses for MP at 550°C (heating rate of 15 K/min and 20 minutes holding time at peak temperature) were conducted. The average volatile content was determined to be 63.8 % on a dry ash-free basis, which is even a lower figure than that obtained with the ISO 562 method at 550°C. TGA for MP at 900°C (heating rate of 10 K/min and 20 minutes holding time at peak temperature) gave a volatile yield of 85.9 % on a dry ash-free basis.

Thermogravimetric analyses for PSD at 550°C and 900°C (heating rate of 10 K/min and 20 minutes holding time at peak temperature) gave 87.3 % and 91.8 % volatile yields on a dry ash-free basis, respectively.

4.4.4 Volatile content measured with LFRD

The volatile contents of MP and PSD were determined with the LFRD according to the following procedure:

The prepared fuel samples were dried in an electric oven at 105°C for 24 hours. Afterwards, one sample was placed in a screw feeder fuel silo and the total weight of the silo was measured. The reactor was heated to a set temperature and flash pyrolysis took place when the fuel particles passed through the 0.5 m-long heated reactor part. During the tests, a fuel feeding rate of 0.07-0.1 g/h was used.

During the measurements, a constant nitrogen flow of 0.3 l/min was used while varying the target temperature level between 550°C and 900°C. The incoming nitrogen flow was stabilized at 20°C, while the cooling and metallic cover parts were kept at a temperature of 200°C.

After each measurement, the fuel silo and the particles collected from the metallic filter were weighed. The mass fraction of volatiles released was calculated as:

$$V = (1 - \frac{m_p}{\Delta m_{silo}}) \quad (4.4)$$

Here m_p is the mass of particles collected and Δm_{silo} is the weight loss of the fuel silo.

Each test point was measured 10 times and the average value was selected as the actual result. Then, the collected particles were further treated in a small furnace according to the ISO 562 standard and loss of mass was measured. Finally, the ash content of the char was measured.

Test results

In general, as the temperature level rose, the volatile yield increased. Furthermore, the test procedure proved to be easily reproducible and the variation between the results was small as the standard deviation in the different test series varied only between 0.2 % - 0.6 %. The complete results are presented in Table 4.4.

Table 4.4. Total volatile release on dry ash-free basis.

Fuel	*550°C*	*700°C*	*800°C*	*900°C*
MP	77.6 %	81.5 %	85.1 %	87.8 %
PSD	90.9 %	95.7 %	96.7 %	-

At highest temperature levels, the ISO 562 standard test increased the volatile yield by only a few percent on a dry ash-free basis. At 550°C, the increase was more significant.

4.4.5 Comparison of results

When the results for peat are compared, the highest volatile yield was measured with the LFRD combined with the ISO 562 test at 900°C, i.e. 87.8 % on a dry ash-free basis. TGA at 900°C gave almost the same result as tests done with LFRD at 800°C. The standardized laboratory tests done at TUT and in a

commercial laboratory gave practically the same volatile yields, i.e. 71.7 % and 71.6 %, respectively, for the studied milled peat.

When the ISO 562 standard was applied at 550°C, it gave an average volatile yield of 66.8 %, while the TGA analysis at the same temperature gave the lowest yield, i.e. only 63.8 %. A summary of tests for MP is presented in Figure 4.12.

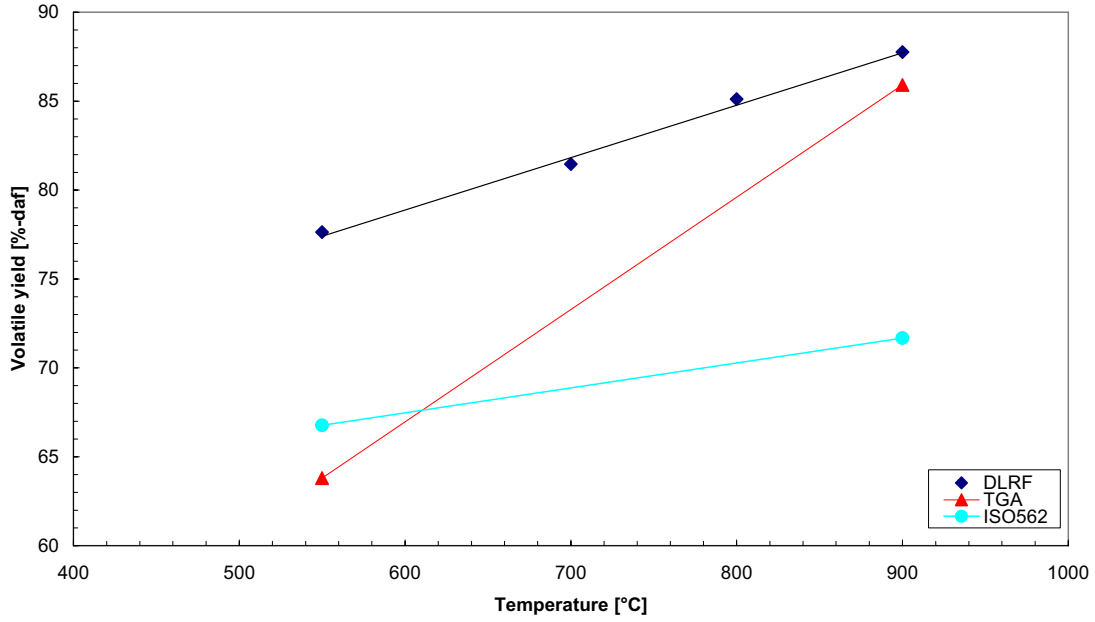

Figure 4.12. Comparison of methods for MP.

The same trend in results can be seen in the case of PSD. The LFRD gave the highest yield, i.e. 96.7 % on a dry ash-free basis at 800°C. The yield at 900°C was not tested. However, the TGA done at 900°C and the LFRD test done at 800°C showed a significant difference in this case. On the other hand, the difference between LFRD and TGA results at 550°C was smaller than in the case of peat. Still, the standardized method gave the lowest yield. A summary of tests for PSD is presented in Figure 4.13.

In summary, when different methods are compared, the LFRD combined with the ISO 562 test provided the highest volatile yield in all test points, regardless of the temperature level. The results also showed that the flash pyrolysis of biomass

produces more volatiles that slow pyrolysis at the same temperature, as reported earlier by Bharadwaj et al. (2004) and by Li et al. (2004).

The large differences between the LFRD and other methods may be attributed mostly to the difference in heating rate (Zanzi et al., 1996) (Li et al., 2004) (Bharadwaj et al., 2004). TGA gave higher volatile yields than standardized methods in almost all cases, which is mainly due to the longer residence time in peak temperature.

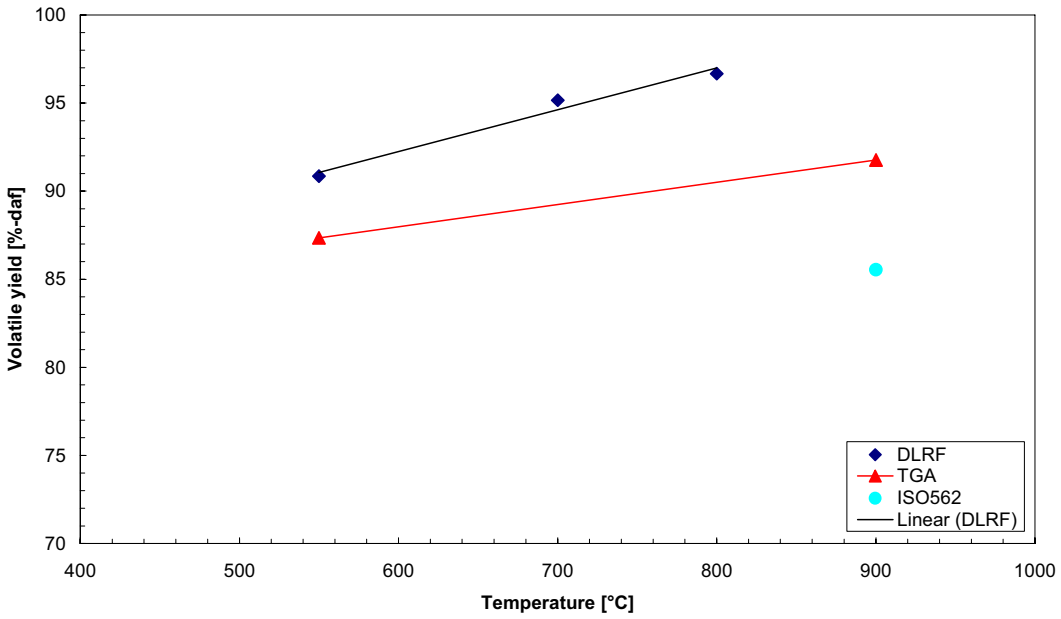

Figure 4.13. Comparison of methods for PSD.

However, as reported earlier in the literature, TGA and other slow-heating-rate methods should only be used for a preliminary fuel characterization. Methods that have conditions more similar to those of practical applications should be used for more accurate fuel characterization (Wiktorsson and Wanzl, 2000) (Bharadwaj et al., 2004) (Biagini et al., 2005). Furthermore, in analysing the results it becomes obvious that 550°C is not high enough for determination of the volatile content of peat or of any other high-volatile-content solid fuel, regardless of the method used.

4.5 Pyrolysis tests for modeling

In order to determine the proper kinetic parameters for the peat, the pyrolysis of MP (analysis given in Table 4.3) was studied in built reactors following the guidelines of the procedure presented in Section 4.4.4. Two different particle sizes were prepared and fed to the hot reactors at two different temperatures and with two different nitrogen flows. In the following results, a particle size of 100-125 μm is noted as "small" and a particle size of 180-225 μm is noted as "big".

Table 4.5 presents the volatile yields on a dry ash-free basis obtained from experiments. The test method was shown to give repeatable results, as the standard deviation of every single test point was less than 0.8 %, the average being 0.5 %. The further treatment of char particles according to the standard ISO 562 increased the volatile yield for both particle sizes by 2-3 % on a dry ash-free basis.

Table 4.5. Volatile yields of MP on dry ash-free basis using LFRD only.

Reactor length [cm]	*Nitrogen flow* [l/min]	*Volatiles at 800°C* "small" [%-daf]	"big" [%-daf]	*Volatiles at 700°C* "small" [%-daf]	"big" [%-daf]
50	0.3	87.9	84.4	79.4	76.4
50	0.7	87.6	83.1	78.7	76.0
30	0.3	87.5	83.5	79.0	74.3
30	0.7	83.0	75.6	75.0	68.5
15	0.7	60.1	50.4	55.1	48.0

To determine the maximum volatile matter of MP, one test series with "small" particles was carried out in a reactor of length 0.5 m with a nitrogen flow of 0.3 l/min at the temperature of 1100°C. The volatile yield obtained on a dry ash-free basis was 91.6 %.

The bulk density of the peat was measured to be 705 kg/m^3.

CHAPTER 5

Model calculations

In this chapter, the pyrolysis model, a straightforward method for determining the kinetic parameters from experimental data and the modeling results are presented. Additionally, some key parameters influencing the modeling results are discussed.

5.1 Pyrolysis model

For the pyrolysis of MP, the equation of motion is provided by Equation 2.28 and the equation of energy by Equation 2.51:

$$\frac{d\vec{v}_p}{dt} = \frac{3}{4}\frac{C_D \rho_g}{d_p \rho_p}\left(\vec{v}_g - \vec{v}_p\right)\left|\vec{v}_g - \vec{v}_p\right| + \frac{\rho_p - \rho_g}{\rho_p}\vec{g} \tag{2.28}$$

$$\rho_p c_p \frac{\partial T}{\partial t} = \frac{1}{r^2}\frac{\partial}{\partial r}\left(\lambda_p r^2 \frac{\partial T}{\partial r}\right) - c_{vol}\dot{m}''_{vol}\frac{\partial T}{\partial r} + q_{pyr}\frac{\partial \rho_p}{\partial t} \tag{2.51}$$

The mass flux of the volatile compounds is given by Equation 2.52. The kinetics of the pyrolysis was modeled using two different models. The one-reaction model is given by Equation 2.53. The two-competing-reactions model is given by Equations 2.54-2.56.

In the two-competing-reactions model, the value of 64 % on a dry ash-free basis for y_1 was selected on the grounds of the thermogravimetric analyses presented in Section 4.4.3 done at 550°C for MP. The value for y_2 was determined using Equations 2.21 and 2.22.

The specific heat and thermal conductivity of a particle were modeled using correlations given by Merrick in Sections 2.9.2 and 2.9.3, respectively. These properties were calculated using transient mass fractions of un-reacted fuel and char. The generated ash is assumed to remain in the char. The transient specific heat was calculated as follows, where the values for $c_{p,act}$ and $c_{p,c}$ were calculated using Equation 2.43:

$$c_p = \gamma_{act} c_{p,act} + \gamma_c c_{p,c} \tag{5.1}$$

The transient thermal conductivity was calculated similarly as follows, where the thermal conductivity for un-reacted fuel was calculated using Equation 2.49 and the thermal conductivity for char was calculated using Equation 2.50:

$$\lambda_p = \gamma_{act} \lambda_{p,act} + \gamma_c \lambda_{p,c} \tag{5.2}$$

The constant-diameter model was adopted on the basis of the work of Biagini et al. (2005), who studied the devolatilization of coal and hazelnut shells in an entrained flow reactor. They reported quite good results with both constant-density and constant-diameter models, but when the temperature range of 973-1073 K was studied in more detail, the constant-diameter model seemed to provide slightly better results. However, at higher temperatures both models gave similar results, with no significant differences. Therefore, using a constant-diameter model, mass loss is described as a loss of density, as presented in Equation 2.38.

In the one-reaction model, the transient mass fractions and the density of the un-reacted fuel were calculated using the known initial density ρ_0 and the known final density ρ_∞ as follows:

Before pyrolysis: After pyrolysis:

$$\begin{aligned} \rho_{act}(0) &= \rho_0 \\ \rho_c(0) &= 0 \\ \rho_p(0) &= \rho_0 \end{aligned} \qquad \begin{aligned} \rho_{act}(t) &= 0 \\ \rho_c(t) &= \rho_\infty \\ \rho_p(t) &= \rho_\infty \end{aligned} \tag{5.3}$$

$$\rho_{act} = \frac{\rho_p - \rho_\infty}{1 - \rho_\infty / \rho_0} \tag{5.4}$$

$$\gamma_{act} = \frac{\rho_{act}}{\rho_p} \tag{5.5}$$

$$\gamma_c = 1 - \gamma_{act} \tag{5.6}$$

In the two-competing-reactions model, the transient mass fractions of un-reacted fuel and char were calculated from Equations 2.54-2.56, and the density of the fuel particle was calculated as:

$$\rho_p = \rho_{act} + \rho_c \tag{5.7}$$

The specific heat of the volatile compounds was modeled using correlations for the air (Incropera and DeWitt, 1996) and the thermal conductivity and dynamic viscosity of nitrogen were calculated using the correlations presented by Incropera and DeWitt (1996).

The reaction enthalpy of the devolatilization reactions was modeled as endothermic. In this case, a constant value 250 $kJkg^{-1}$ was chosen, based on the work of Aho et al. (1989).

On the basis of the results presented in Figure 4.10, the following correlation for drag coefficient was used:

$$C_D = \frac{96}{\mathrm{Re}_p^{1.3}} \cdot e^{-B} \tag{5.8}$$

On the grounds of the particle position measurements presented in Section 4.3.5, the gas velocity in the reactor for the studied fuel particle was modeled to be 96.5 % of the maximum velocity.

In the modeling, the initial and boundary conditions presented in Equations 2.57-2.59 and in Equation 2.62 were used. A particle emissivity value of 0.9 was chosen. The reactor parts 3, 4 and 5 presented in Figure 4.1 were included in the pyrolysis model. The temperature profiles of the reactor were modeled according to the results presented in Section 4.2.1.

The experimental data for modeling is presented in Section 4.5. Average particle sizes used in modeling were 120 μm and 200 μm for “small” and “big” notations, respectively.

Furthermore, the following hypotheses were used in the modeling:

- The fuel particle is dry, spherical and isotropic.
- Char does not deform or change size during pyrolysis.
- Volatile compounds flow outwards from the particle immediately after forming and are in thermal equilibrium with solid matter.
- No secondary reactions occur between volatile compounds and solid matter.
- Flow of volatile gases does not change the velocity of the particle.
- Constant pressure of surrounding gas.
- Radiant heat transfer takes place only between reactor walls and particle.
- Thermal conductivity and dynamic viscosity of the gas depend only on the temperature.

5.2 Solving of kinetic parameters

A simple and straightforward method for determining the kinetic parameters from experimental data is presented in Figure 5.1. The aim of the method is to combine in one entity both one- and two-reaction models and the results obtained with two different particle sizes.

In the scheme below, “low” parameters refer to the kinetic parameters governing the low-temperature reactions (related to k_1 in Equations 2.54-2.56) and these parameters were solved using the results obtained from tests with “big” particles. Accordingly, “high” reaction refers to the parameters governing the high-temperature reactions (related to k_2 in Equations 2.54-2.56) and these parameters were calculated using the results obtained from tests with “small” particles.

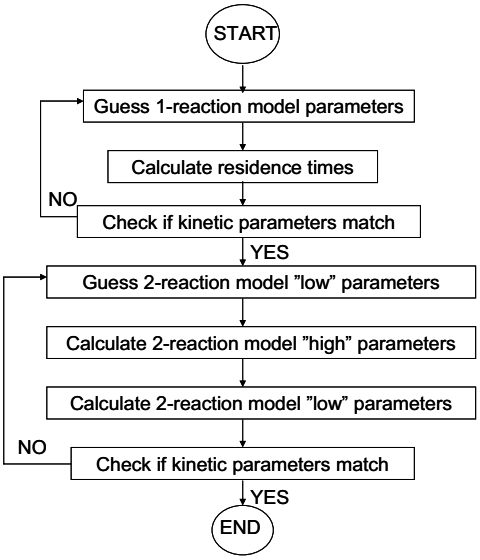

Figure 5.1. Scheme for solving kinetic parameters.

The process starts by guessing the kinetic parameters for the one-reaction model, which is used for solving the particle residence times in the reactor for both particle sizes and all test points. As the distance a particle travels (i.e. the lengths of the heated and cooling parts of the reactor) and the mass loss of the particle are known, the residence time in the reactor can be calculated.

Next, the kinetic parameters are determined from the received residence time-volatile yield data and the process is repeated until the guessed and calculated parameters fit.

Then, the “low” reaction parameters for the two-competing-reactions model are guessed and “high” reaction parameters are solved from data obtained from tests with “small” particles.

Finally, the “low” reaction parameters are calculated from data on “big” particles. If the guessed and solved parameters do not match, the iteration starts again with a new guessing of “low” parameters.

5.3 One-reaction model results

According to the scheme presented in Figure 5.1, the process started with guessing the kinetic parameters of the one-reaction model. By carrying out the iterative process described in Section 5.2, the following kinetic parameters were obtained for the one-reaction model:

Table 5.1. Calculated kinetic parameters for one-reaction model.

One-reaction model		*“small”*		*“big”*	
		A [s^{-1}]	E [$Jmol^{-1}$]	A [s^{-1}]	E [$Jmol^{-1}$]
800°C	“uniform”	1.00E+5	8.20E+4	1.00E+5	8.20E+4
800°C	“non-uniform”	1.00E+5	8.20E+4	1.00E+5	8.05E+4
700°C	“uniform”	1.00E+5	7.45E+4	1.00E+5	7.45E+4
700°C	“non-uniform”	1.00E+5	7.45E+4	1.00E+5	7.40E+4

In Table 5.1, the results marked “uniform” were modeled using uniform temperature inside the particle, i.e. there were no temperature gradients inside the particle. The parameters marked “non-uniform” were modeled using the thermal conductivity model described in Section 5.1.

With the kinetic parameters presented in Table 5.1, the following residence times presented in Table 5.2 were obtained for particles inside the reactor:

Table 5.2. The calculated residence times for MP particles.

		Residence time points [s]				
		1	2	3	4	5
800°C	“small”	0	0.35	0.54	0.86	1.24
800°C	“big”	0	0.31	0.47	0.78	1.19
700°C	“small”	0	0.38	0.59	0.94	1.35
700°C	“big”	0	0.33	0.51	0.85	1.28

The fitting of kinetic parameters based on the least squares method to the measured data points (residence time-mass loss) is illustrated in Figure 5.2.

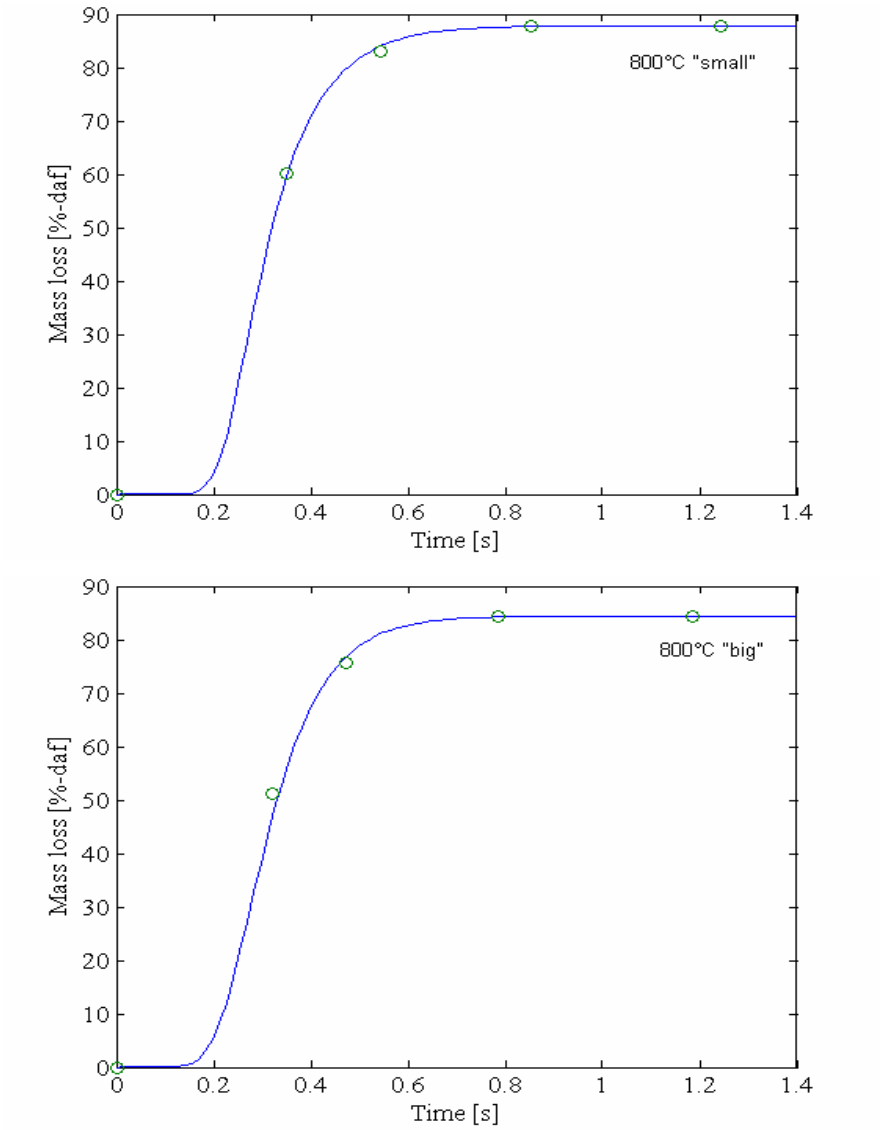

Figure 5.2. Fitting of kinetic parameters (line) to measured data points (dots).

When the kinetic parameters in Table 5.1 are re-examined, it can be seen that the frequency factor remains constant and that only the activation energy changes. However, both the “uniform” and the “non-uniform” cases of “small” particles were modeled with the same set of kinetic parameters at both temperature levels. When the temperature level was raised, the activation energies increased roughly by 10% for both “uniform” and “non-uniform” models. For reference, the values A= $1 \cdot 10^5$ s^{-1} and E=80 $kJmol^{-1}$ have been used by Saastamoinen et al. (1993) as kinetic parameters for pyrolysis in the modeling of pulverized peat combustion at 850°C. It is also interesting to compare the activation energies determined in this work with values presented for some biomass fuels in the literature. It should be noted that the apparent activation energies determined in this study for MP are significantly greater that those presented in Table 5.3, which vary from 32 to 49 $kJmol^{-1}$ for four biomass fuels at high heating rate.

Table 5.3. Kinetic parameters for four biomass fuels (Shuangning et al., 2006).

Raw material	*A ·10^3 (s^{-1})*	*E ($kJmol^{-1}$)*
Wheat straw	1.05	31.65
Coconut shell	6.84	48.73
Rice husk	1.19	39.30
Cotton stalk	2.44	40.84

When the relative importance of internal and external heat transfer mechanisms was studied with the heat transfer Biot number introduced in Section 2.4.2, it was found that the Biot number was less than one in all modeled test points. Biot numbers in modeled test points are presented in Figure 5.3.

On the basis of the modeled Biot numbers, pyrolysis took place in the intermediate zone, i.e. the internal heat transfer was fast, but not so fast that a particle could directly be assumed to be practically at uniform temperature. Therefore, the relative importance of internal processes was further studied using the pyrolysis number, also introduced in Section 2.4.2.

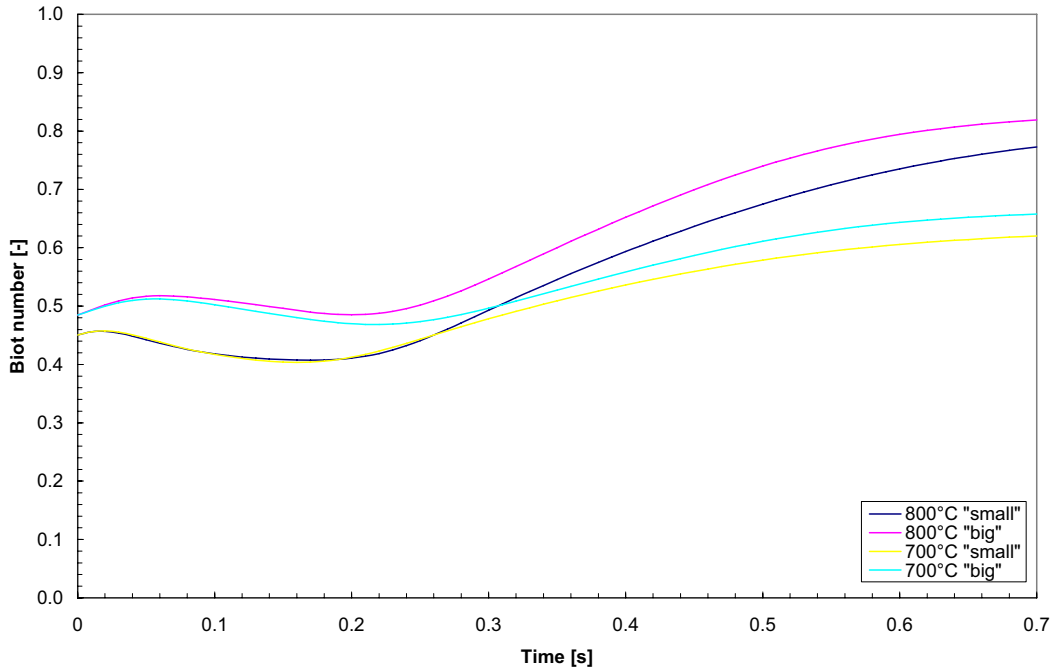

Figure 5.3. Biot numbers in modeled test points.

The analysis showed that in all test points the pyrolysis number was > 1, which means that both chemical kinetics and internal heat transfer should be taken into account. Pyrolysis numbers in the modeled test points are presented in Figure 5.4.

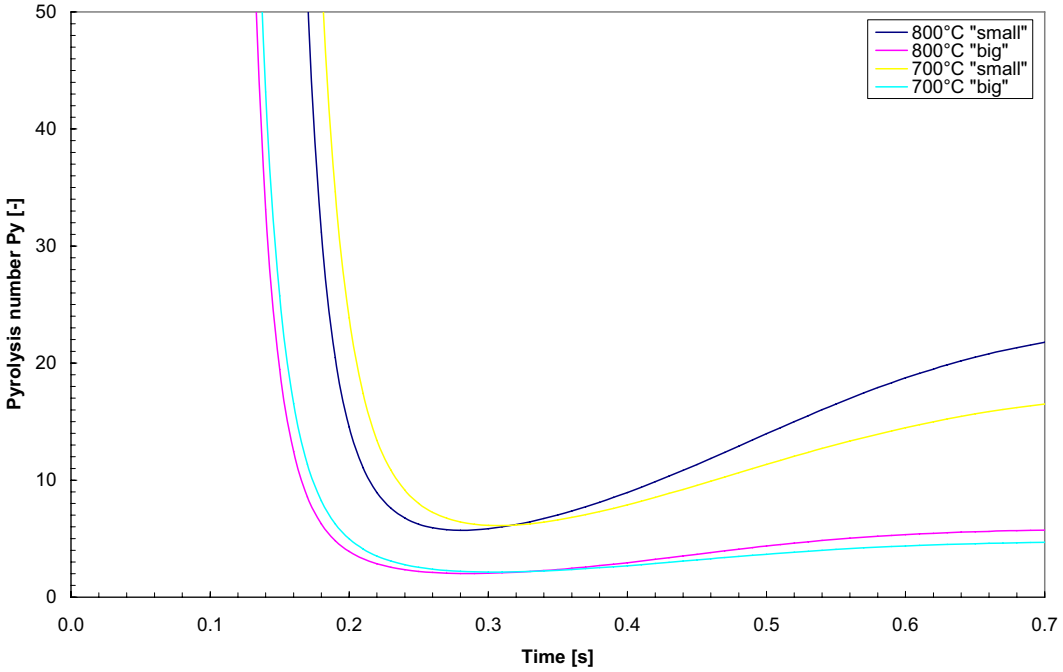

Figure 5.4. Pyrolysis numbers in modeled test points.

Based on the analysis of both Biot and pyrolysis numbers of the test points (*Bi<1* and *Py>1*), it was concluded that a thermal conductivity model should be included in further analysis. Consequently, the one-reaction model including the thermal conductivity model and 10 internal zones for a particle was applied to test points, and temperature profiles inside the particles were calculated. Examples of the temperature profiles are presented in Figure 5.5.

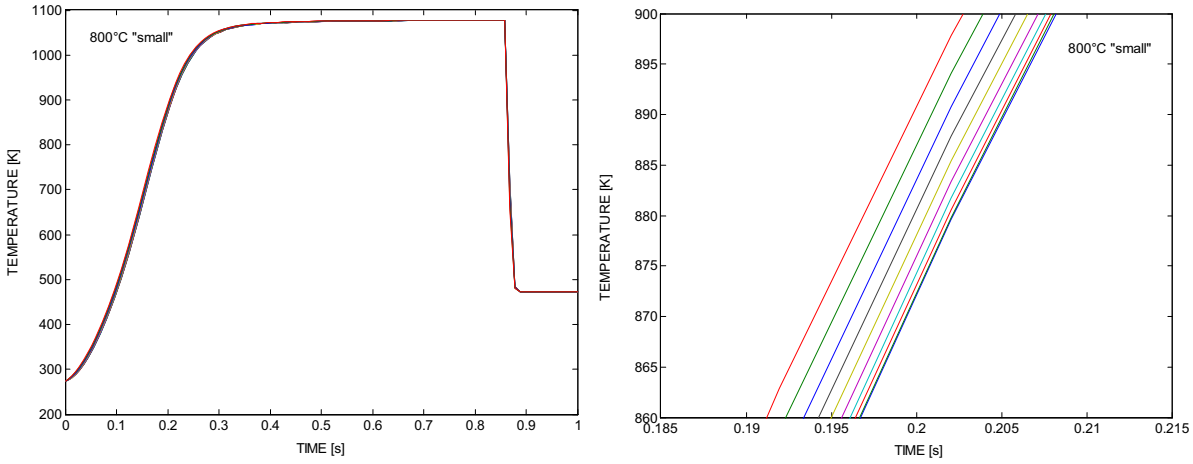

Figure 5.5. Temperature profile of “small” particle at 800°C.

In Figure 5.5, the small picture on the left side represents the temperature profile of a fuel particle inside the reactor. The picture on the right is a zoomed example of the picture on the left to illustrate the temperature gradients inside the fuel particle. To further demonstrate the importance of thermal conductivity, the temperature differences between the centre and the surface of the fuel particle in modeled test points are plotted in Figure 5.6.

Figure 5.6 shows that temperature differences were at worst close to 70°C in the case of “big” particles, which justified the use of the thermal conductivity model. On the other hand, the temperature differences were smaller in the case of “small” particles, which on the basis of the modeling results might be modeled with a uniform particle temperature model without causing any big error. Furthermore, “small” particles were modeled with the same set of kinetic parameters, regardless of the model, which again shows that the temperature

differences inside the particle are not a source of big error in the case of “small” particles.

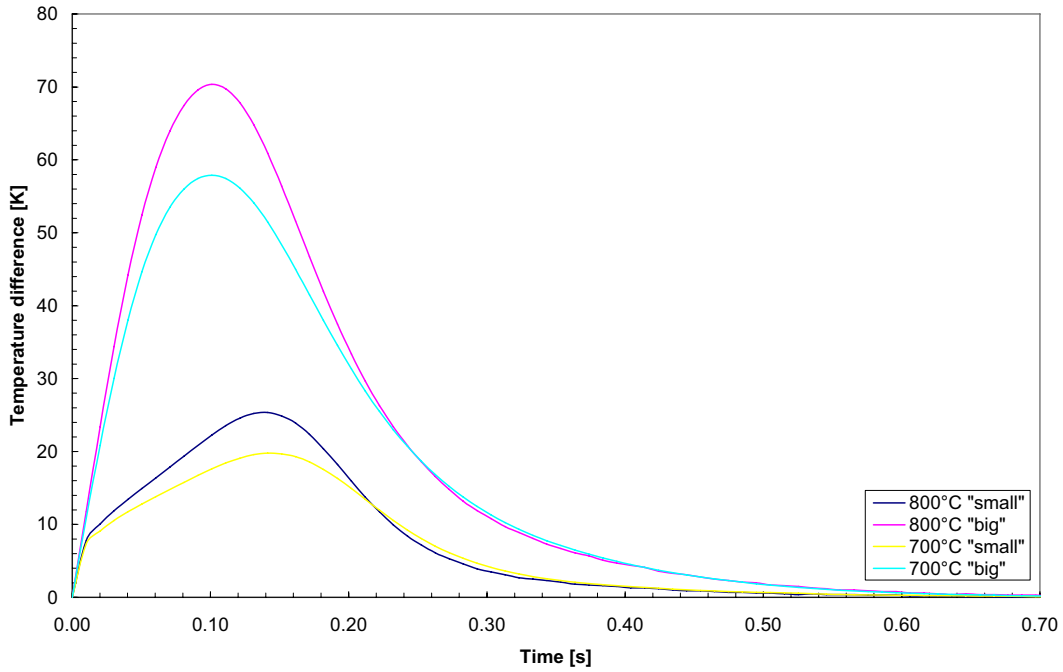

Figure 5.6. Temperature differences of centre and surface of particle.

5.4 Two-competing-reactions model results

The solving process presented in Figure 5.1 was continued by solving the kinetic parameters for the two-competing-reactions model. By continuing the iterative process, the following kinetic parameters presented in Table 5.4 were obtained for the two-competing-reactions model while using the thermal conductivity model and 10 internal zones for a particle:

Table 5.4. Calculated kinetic parameters for two-competing-reactions model.

Two-competing-reactions model		y_1	y_2	*"low"* A [s^{-1}]	*"low"* E [$Jmol^{-1}$]	*"high"* A [s^{-1}]	*"high"* E [$Jmol^{-1}$]
800°C	"small"	0.64	0.92	1.93E+2	4.79E+4	1.25E+5	8.57E+4
800°C	"big"	0.64	0.88	1.93E+2	4.79E+4	1.25E+5	8.57E+4
700°C	"small"	0.64	0.85	4.77E+2	4.67E+4	1.30E+5	8.00E+4
700°C	"big"	0.64	0.82	4.77E+2	4.67E+4	1.30E+5	8.00E+4

When the kinetic parameters in Table 5.4 are examined, it can be seen that the same set of kinetic parameters now fit both particle sizes at one temperature level; only y_2 is changed according to particle size. Furthermore, it can be seen that the parameters of the "high" reaction change with increasing temperature similarly to the one-reaction model parameters, i.e. the frequency factor remains practically the same and activation energy increases roughly by 10%. The frequency factor of the "low" reaction drops 60% as the temperature increases, whereas the increase in activation energy is not very significant. It is also worth noticing that the kinetic parameters of the "high" reaction are quite close to those of the one-reaction model.

When the reaction rate constants of the two-competing-reactions model are examined, it can be seen that "low" reaction is the dominant reaction up to the temperature level of 480°C. After that, "high" reaction controls the rate of pyrolysis in modeled cases. An example of reaction rate constants is plotted in Figure 5.7. In Figure 5.7, the blue line represents the reaction rate of "low" reactions, the green line represents the reaction rate of "high" reactions and the red line is the combined reaction rate constant.

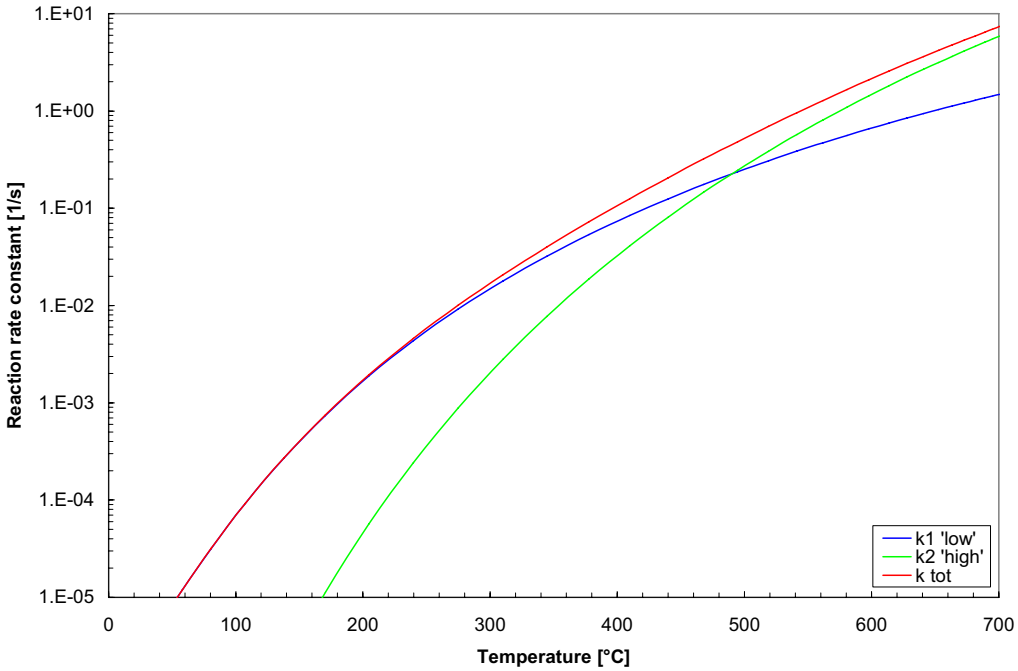

Figure 5.7. Reaction rate constants during modeling.

5.5 Discussion

In the following, the effects of some key parameters on the results of pyrolysis modeling are discussed. Also, a method for estimating final volatile yield of peat pyrolysis is presented and the heating rates during the tests are calculated.

5.5.1 Particle size distribution

The kinetic parameters for the one-reaction and two-competing-reactions models presented in Tables 5.1 and 5.4 were calculated using one average particle size which represented the whole particle size distribution range. However, using the same kinetic parameters, also the mass loss curves can be calculated for both maximum and minimum sizes of the particle size distribution. Examples of these mass loss curves are presented in Figure 5.8.

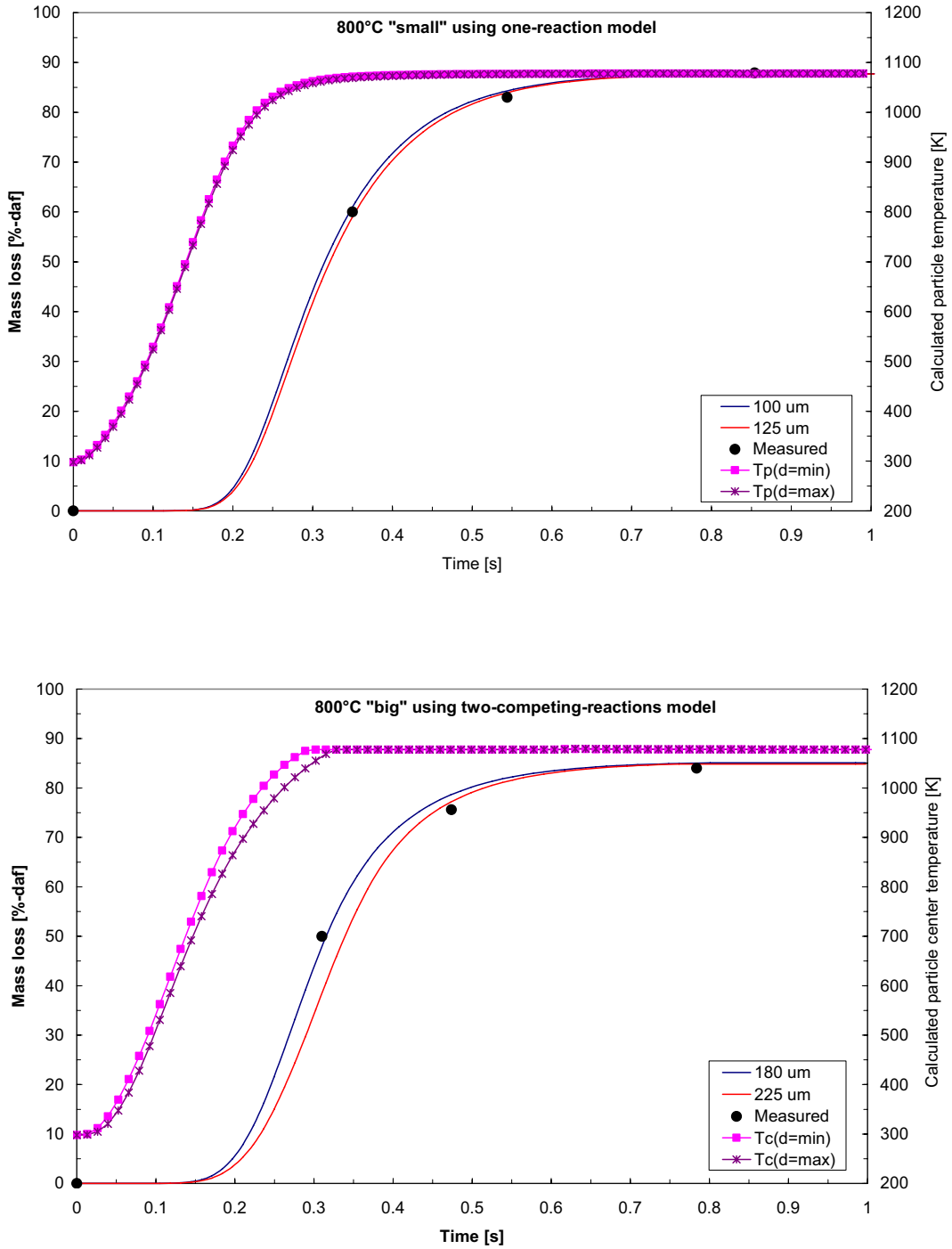

Figure 5.8. Mass loss curves calculated for minimum and maximum particle sizes using one-reaction and two-competing-reactions models.

It can be seen from Figure 5.8 that with a small particle size distribution range, which is the case with “small” particles, both mass loss as well as the particle temperature curves for minimum and maximum particle size are close to each

other and one average particle size can be used for the determination of kinetic parameters without this leading to any great error in modeling results. However, with a bigger particle size distribution range, which is the case with “big” particles, minimum and maximum particle size mass loss curves have big differences, especially in the areas of strongest pyrolysis. Using a big particle size distribution range and one average particle size might lead to difficulties in interpreting the measured data, especially in the middle part of the mass loss curve where the differences are significant. It is also possible with big particle size distribution that in the last part of the mass loss curve only the biggest particles are reacting since the smallest particles have already finished reacting, which causes some inaccuracy in the calculated results. In general, if both the minimum and maximum particle sizes increase, also the effect of internal heat transfer could make the interpretation of experimental results more difficult.

The use of one average particle size in cases which include a big particle size fraction could be avoided by dividing the original particle size fraction into smaller sub-fractions and by calculating mass loss curves for each sub-fraction. The final mass loss curve can be constructed from each sub-fraction curve by calculating the mass-fraction-based weighted average. Saastamoinen et al. (2006) found that a comparison of the mass loss of single-size particle with the mass loss of a big particle size fraction shows that the mass loss curve becomes wider and not so steep for the big particle size fraction.

5.5.2 Fuel thermal properties

As noted in Section 2.9, fuel thermal properties have a significant effect on the course of pyrolysis. The change in specific heat in the test points during pyrolysis according to the Merrick model is presented in Figure 5.9.

When the model presented by Gronli (1996) for biomass as:

$$c_p = 1500 + 1.00 \cdot T \tag{5.9}$$

was substituted for the Merrick model for specific heat and the pyrolysis of “big” particles was calculated using the two-competing-reactions model at 700°C and 800°C with 10 internal zones, it was found that the temperature differences inside a particle increased only a little. The temperature difference between the centre and the surface of a particle using Gronli’s model and the transient mass loss difference between these two models are presented in Figure 5.10.

It can be seen from Figure 5.10 that even though Gronli’s model increases the temperature differences during the heating (see Figure 5.7), this did not have a significant effect on the total mass loss, and therefore both models could be used for modeling the pyrolysis of peat without leading to any great error in the final results.

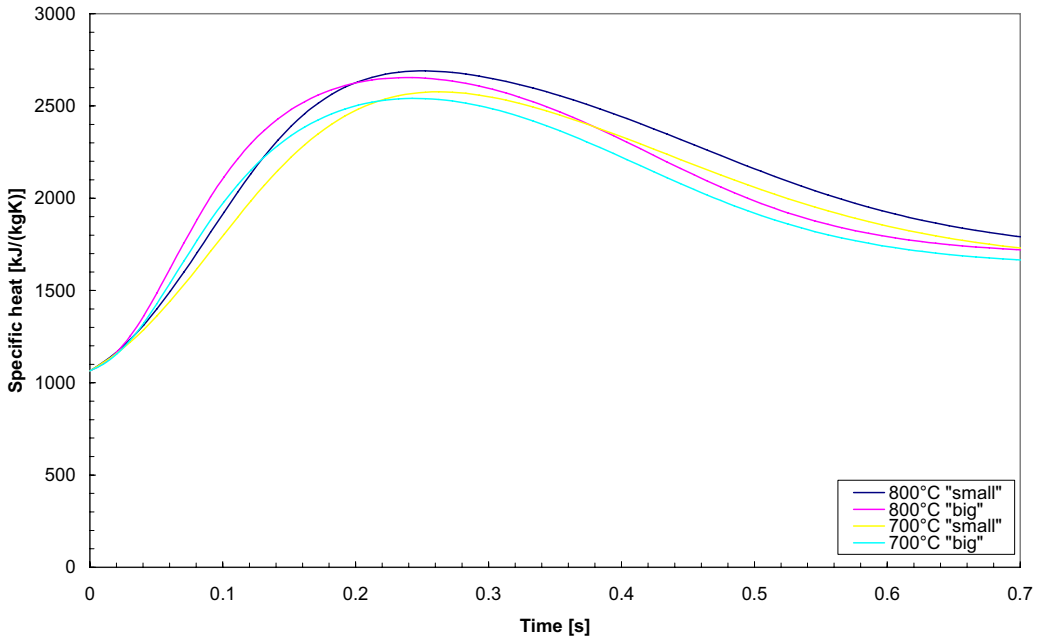

Figure 5.9. Change in specific heat in test points according to Merrick model.

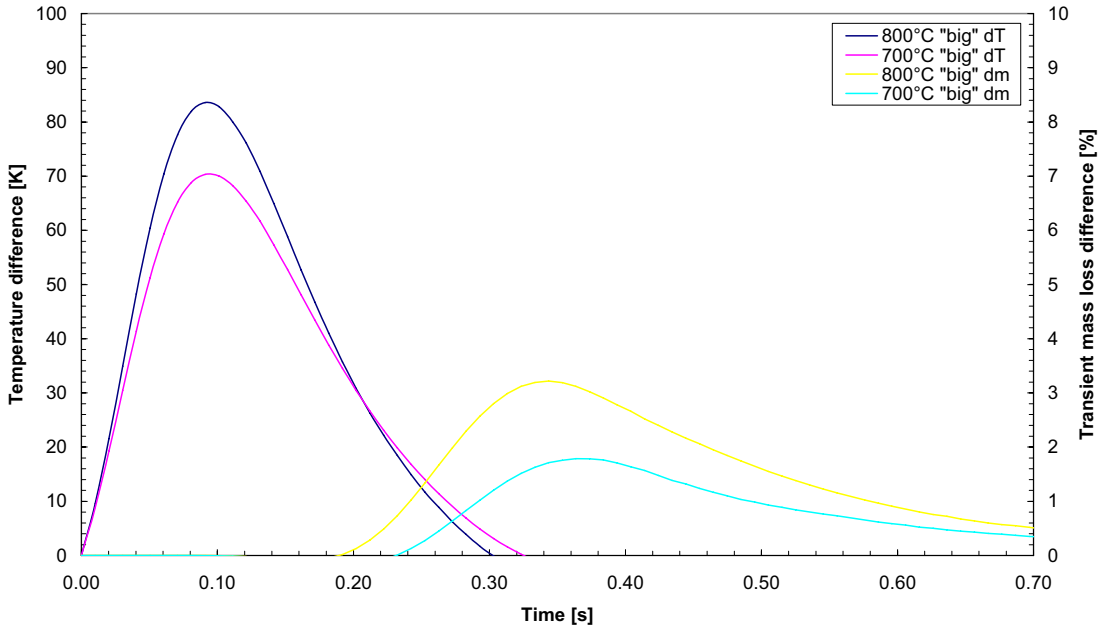

Figure 5.10. Comparison of results of different specific heat models.

The change in specific heat in the test points according to the Merrick model is presented in Figure 5.11. Similarly, when the constant value of

$$\lambda = 0.25 \text{ Wm}^{-1}\text{K}^{-1} \tag{5.10}$$

was adopted for thermal conductivity, as done in the biomass modeling work of Bharadwaj et al. (2004), and the pyrolysis of “big” particles was calculated using the two-competing-reactions model at 700°C and 800°C with 10 internal zones, it was found that the choice of model had no significant effect on the modeling results. The temperature difference between the centre and the surface of a particle using the constant value of 0.25 $\text{Wm}^{-1}\text{K}^{-1}$ for thermal conductivity and the transient mass loss difference between these two models are presented in Figure 5.12.

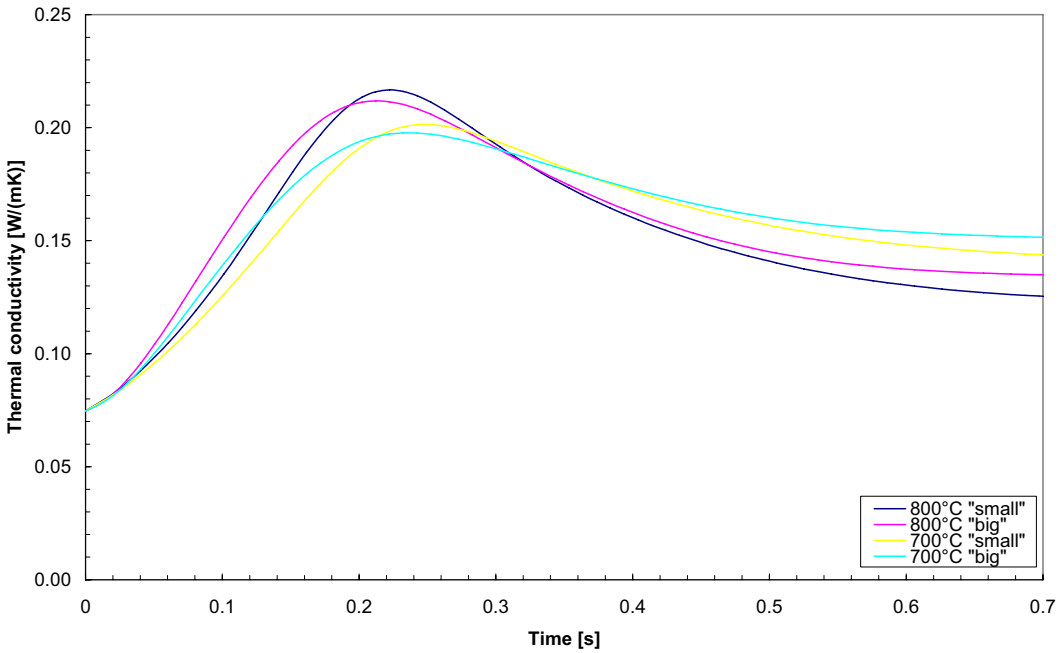

Figure 5.11 Change in thermal conductivity in test points.

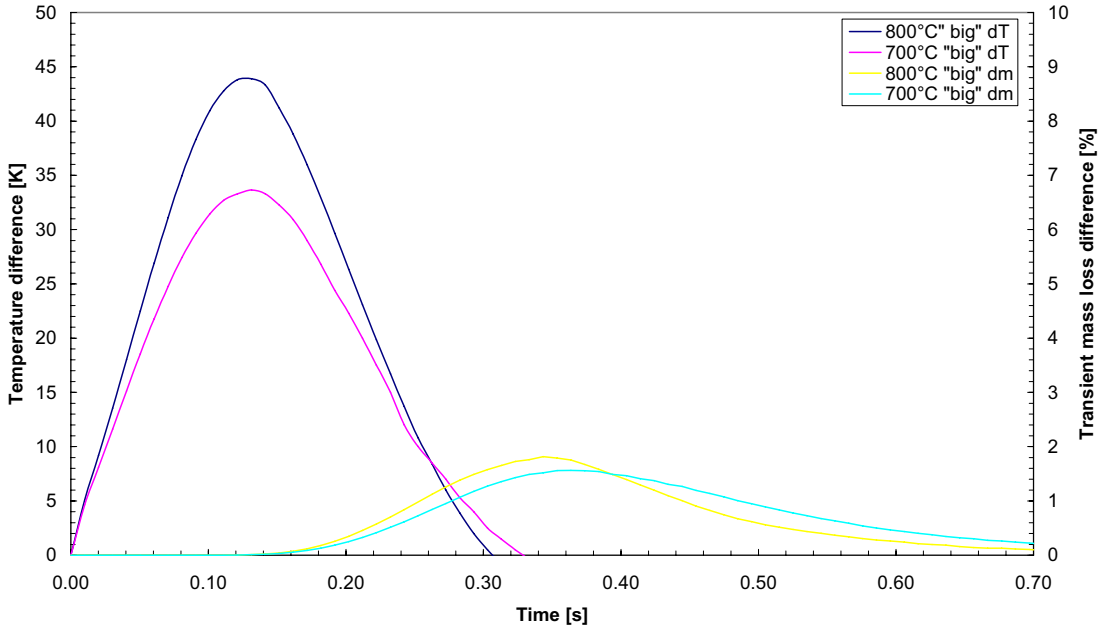

Figure 5.12. Comparison of results of different thermal conductivity models.

When both models presented in Equations 5.9 and 5.10 were used at the same time, the modeling results did not change significantly, as can be seen in Figure 5.13.

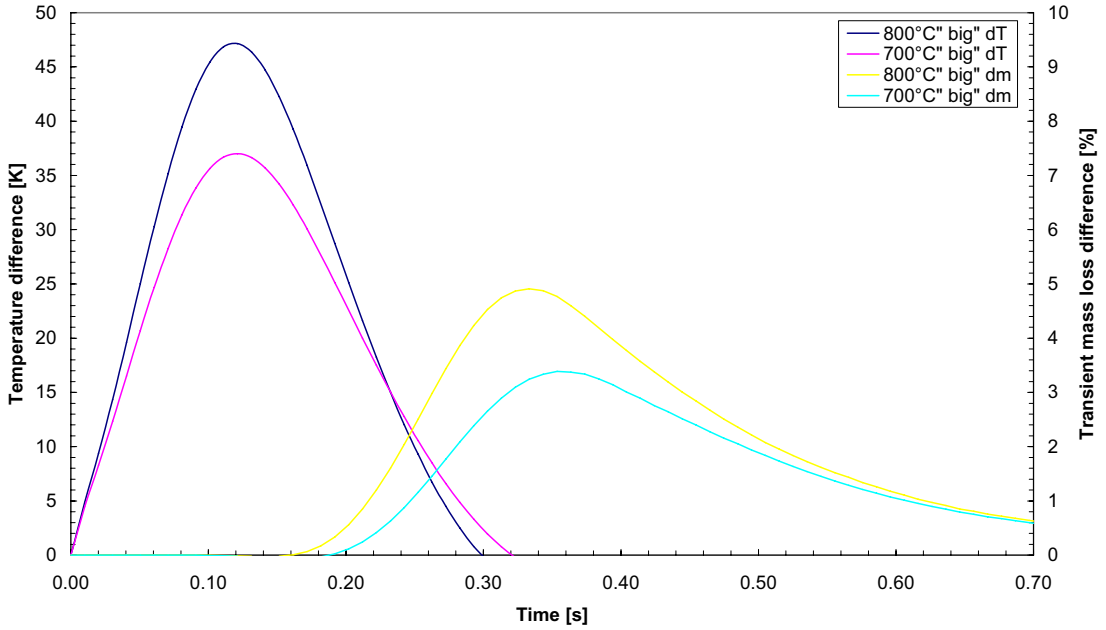

Figure 5.13. Comparison of combined results of different models.

In summary, any combination of specific heat or thermal conductivity models discussed here could be used for modeling the pyrolysis of peat. The selection of models had no significant effect on the modeling results, as the transient mass losses varied less than 5 %.

5.5.3 Drag coefficient

In the modeling, the residence time of a particle inside the reactor is calculated using the equation of motion presented in Equation 2.28. The slip velocity of a particle (i.e. the difference in velocity between the gas and the particle) during the tests is presented in Figure 5.14.

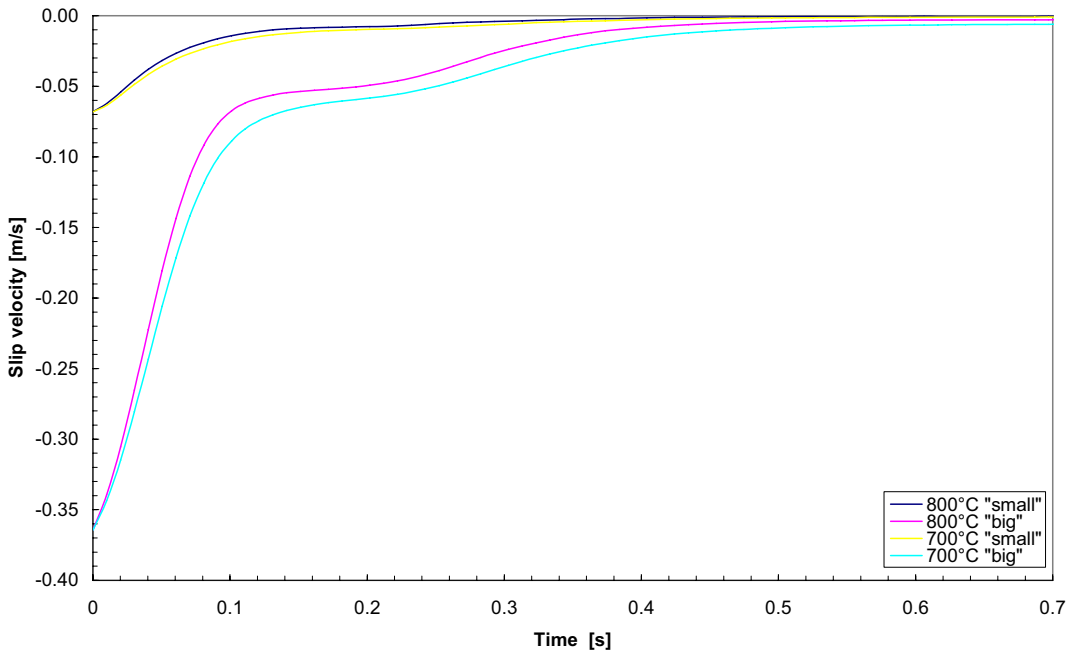

Figure 5.14. Slip velocity of particle during tests.

It can be seen in Figure 5.14 that at the beginning especially “big” fuel particles move significantly faster than the gas, i.e. the reactor could be defined as a drop tube reactor. Therefore, the residence time of a fuel particle inside the reactor cannot be calculated in any circumstances using the gas velocity.

As reported in Section 4.3.5, the measured terminal velocities of peat particles could not be explained using drag coefficient correlations for spherical particles presented in Equations 2.31-2.34. However, if correlations for spherical particles are used, the residence times of fuel particles inside the reactor change significantly. For example, if residence time point 4 in Table 5.2 is examined, the residence times of “small” particles decrease inside the reactor by 0.09-0.10 s, depending on the temperature level, which means an error of over 10 % in the calculated residence times. In the case of “big” particles the error is even greater: the residence times of “big” particles decreased inside the reactor by 0.17-0.21 s, depending on the temperature level, which means an error of over 20 % in the calculated residence times.

The transient velocity ratio v_r of a peat particle can be calculated as:

$$v_r = \frac{v_{sph}}{v_{mea}} \cdot 100\,\% \tag{5.11}$$

where v_{sph} is the transient velocity of the peat particle calculated using correlations for spherical particles and v_{mea} is the transient velocity calculated with the measured correlation given in Equation 5.8. The calculated velocity ratios are presented in Figure 5.15.

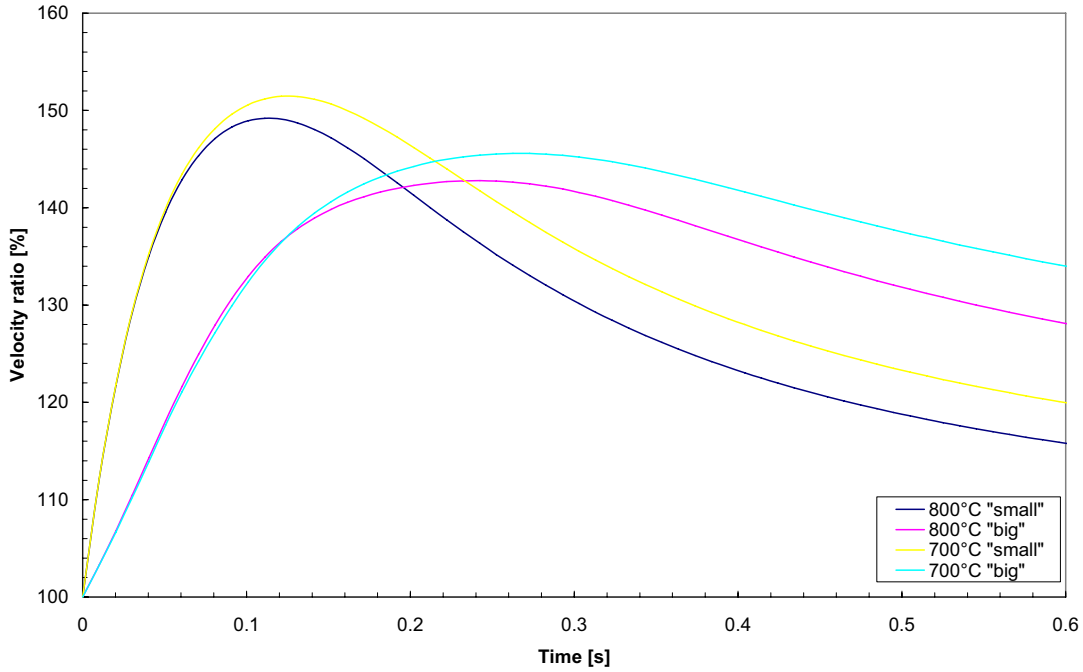

Figure 5.15. Velocity ratios of peat particles calculated with different correlations.

An examination of Figure 5.15 shows that the correlation for spherical particles overestimates the transient velocity of a fuel particle by 50 % at worst. Therefore, it is clear that if a drop tube reactor is used, measurement of the drag coefficient of the fuel studied should be part of the test procedure since the assumption of spherical particles might cause a significant error in residence time calculations. As presented earlier in this dissertation, optical measurement techniques are well suited for this purpose.

5.5.4 Reaction enthalpy

When the reaction enthalpy of the devolatilization reactions was changed from the constant value 250 kJkg^{-1} to the value 120 kJkg^{-1}, this had no significant effect on modeling results. Similar results have been reported earlier, for example by Raiko (1986) and by Solomon et al. (1992).

5.5.5 Method for estimating final volatile yield of peat pyrolysis

Zhang et al. (1990) presented a model for estimating the final volatilie yield of pulverized coal devolatilization. They studied 14 different Chinese coal types in an electric furnace at temperatures between 573-1873 K and constructed a relationship between final volatile yield and ambient temperature. Adopting their approach, the results presented for peat at temperatures between 700-900°C in Table 4.4 were fitted to the relationship presented in Equation 5.12.

$$V_{daf,\infty} = A(V_{prox})^n \exp\left[-B/(T-T_0)^2\right] \quad (5.12)$$

Here $V_{daf,\infty}$ is the final volatile yield, V_{prox} is the amount of volatiles from proximate analysis, T is ambient temperature, T_0 is the reference temperature and A, B and n are fuel-specific constants. The results of the fitting are presented in Table 5.5.

Table 5.5. Calculated parameters for peat pyrolysis compared to original parameters determined for Chinese coal.

Parameter	*Peat*	*Chinese coal (Zhang et al.)*
A	1.28	1.20
B	$8.8 \cdot 10^4$	$2.4 \cdot 10^5$
n	0.80	0.80

The comparison of the results received for the final pyrolysis yield of peat using two different parameter sets presented in Table 5.5 is presented in Figure 5.16.

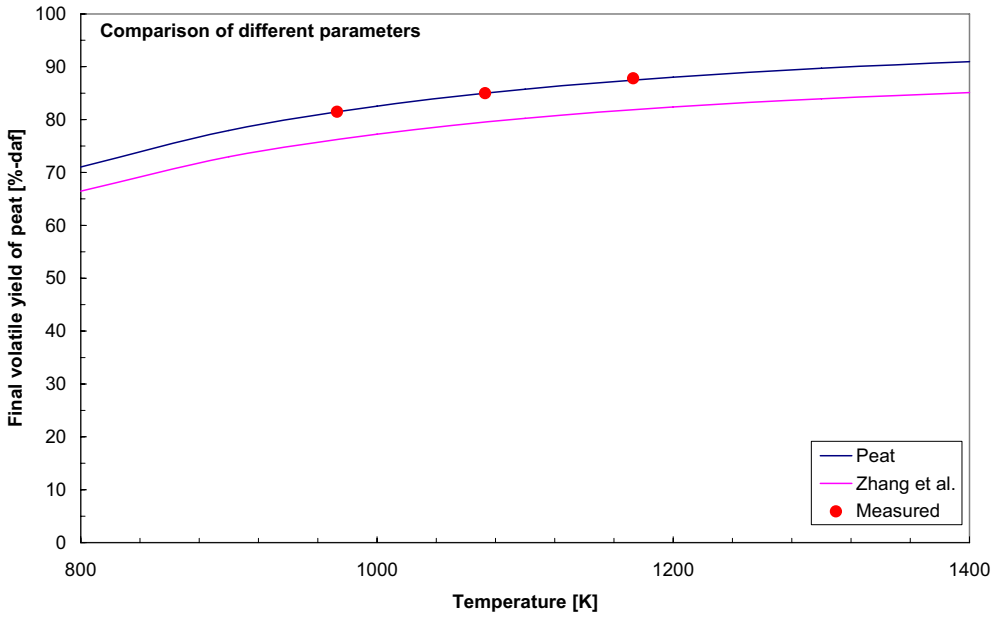

Figure 5.16. Comparison of different parameter sets.

It can be seen from Figure 5.16 that parameters determined for coal predict significantly lower final volatile yields for peat pyrolysis.

5.5.6 Heating rate

One of the most important objectives of this dissertation was to build a high-heating-rate laboratory-scale reactor capable of simulating conditions in FB boilers. To ensure the achievement of this objective, the heating rates during the tests were calculated. The results are presented in Figure 5.17.

When these heating rates are compared with the information given in Table 3.1, it is seen that the reactor can provide heating rates similar to those of the HWM. Therefore, as stated for the HWM, the LFRD is quite well-suited for simulating the conditions in FB boilers.

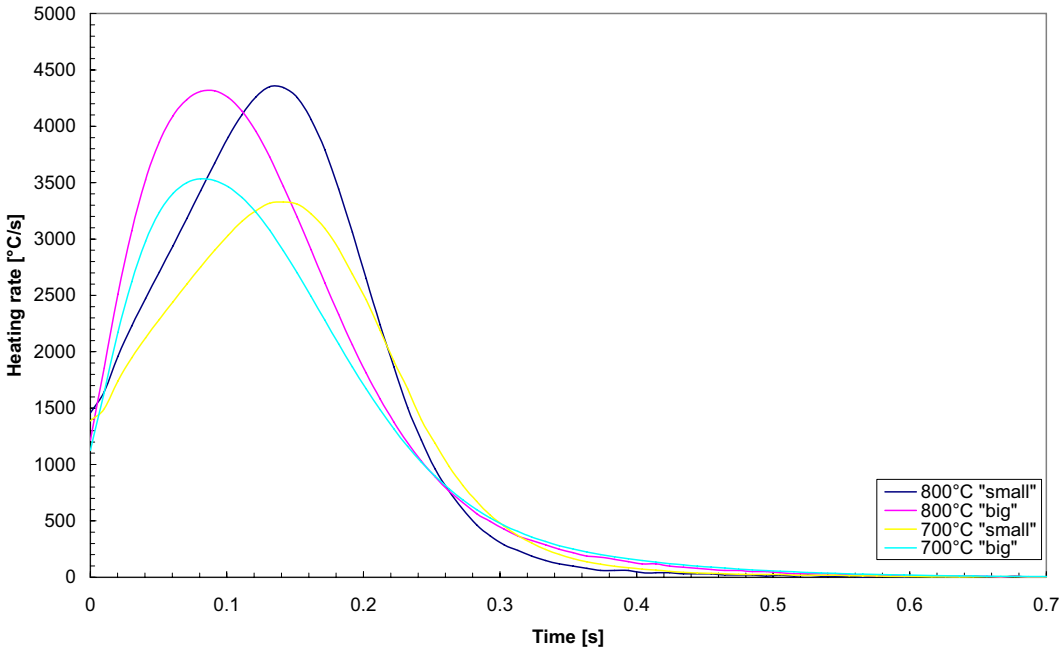

Figure 5.17. Heating rates during test points.

CHAPTER 6

Concluding remarks

In this final chapter, the conclusions from this dissertation are summarized and suggestions for future work are given.

6.1 Results and conclusions

6.1.1 Development and characterization of laminar flow reactor

- A laboratory-scale laminar flow reactor developed for determining the volatile content of high-volatile-content fuels was characterized and it was found that
    - The LFRD is well-suited for pyrolysis studies of high-volatile-content solid fuels.
    - The LFRD provided highest volatile yields for Finnish milled peat and pine sawdust fuels when its results were compared with results obtained using other common analysis methods.
    - Big errors in determining the volatile yield can be made if particle cooling is not carried out at high enough temperatures, due to condensation of tars.
    - The LFRD can be used to determine volatile yields of high-volatile-content fuels at different residence times.
    - Optical measurement techniques can be successfully used for characterization of the reactor and fuels used.

6.1.2 Modeling of pyrolysis of Finnish milled peat

- Based on the experimental results, the kinetic parameters for Finnish milled peat were calculated using two different kinetic models.

- A simple and straightforward method for determining kinetic parameters from experimental data was introduced.

- A method for estimating the final volatile yield of peat pyrolysis was presented.

- However, it should be noted that the calculated kinetic parameters as well as the method for estimating the final volatile yield of peat pyrolysis should be used only in conditions similar to those used in this work.

- In the modeling part of the work it was demonstrated that in drop tube reactors the correlation for the drag coefficient of the fuel might be a major source of error. This case-specific factor should be measured for every fuel tested. Optical measurement techniques, for example, can be used for this purpose, as presented in this dissertation.

- The different specific heat and thermal conductivity models used in this dissertation for fuel particles did not significantly affect modeling results, meaning that any of these could be used for modelling the pyrolysis of peat.

- The 100-120 μm milled peat particles modeled in this work could have been approximated using a uniform temperature model without causing significant error.

6.2 Recommendations for future work

6.2.1 Development of laminar flow reactor

- In pyrolysis, the reaction enthalpies are so small that they have no significant effect on the temperature of the particle, which is not the case in char combustion. In char combustion, the reaction enthalpies significantly increase the temperature of a burning particle. Therefore, in order to study char combustion in the LFRD, a particle temperature measurement option is required. This can be arranged by constructing a new reactor from transparent material or by making measurement openings in the existing reactor. Optical measurement techniques, for example, could be used for particle temperature measurement.

- An option for measuring the composition of formed pyrolysis gases is required. FTIR, for example, could be used for this purpose.

6.2.2 Modeling of pyrolysis

- To further improve the accuracy of the pyrolysis model used and to provide more tools for sensitivity analysis, mass transfer and particle swelling/shrinkage models should be developed and included. Furthermore, modeling of aspherical particles should be considered.

- In connection with particle swelling/shrinkage, a step for measuring particle size before and after the pyrolysis experiment should be added to the test procedure. For this purpose, sieving, microscope and optical measurement techniques, for example, could be used.

- If measurements of pyrolysis gas compositions at different residence times are available, kinetic parameters for each gaseous compound could be determined.

- A so-called "n^{th}-order pyrolysis model" could be constructed by comparing the elementary analysis of fuel and the elementary balance of gas compounds formed. The model could describe pyrolysis as the formation of *n* different gaseous species via single first-order reactions. For this purpose, measurements with the LFRD with different particle residence times would be required, including measurements of the composition of the pyrolysis gases formed. However, with the measurement techniques currently available, the construction of such a model would be extremely challenging.

Bibliography

Abbas T., Awais M.M. and Lockwood F.C., An artificial intelligence treatment of devolatilization for pulverized coal and biomass in co-fired flames, *Combustion and Flame*, 132, 305-318 (2003)

Aho M.J., Tummavuori J.L., Hämäläinen J.P. and Saastamoinen J.J., Determination of heats of pyrolysis and thermal reactivity of peats, *Fuel*, 68:9, 1107-1111 (1989)

Aho M.J. and Saastamoinen J.J., Laboratoriomittakaavan palamisen tutkimuksen laitteet ja menetelmät, in *Poltto ja Palaminen* (Ed. Raiko R. et al., in Finnish), International Flame Research Foundation, Finland (2002)

Anthony D.B., Howard J.B., Hottel H.C. and Meissner H.P., Fifteenth Symposium (International) on Combustion, *The Combustion Institute* (1974)

Backreedy R.I., Habib R., Jones J.M., Pourkashanian M. and Williams A., An extended coal combustion model, *Fuel*, 14, 1745-1754 (1999)

Bharadwaj A., Baxter L. and Robinson A., Effects of Intraparticle Heat and Mass Transfer on Biomass Devolatilization: Experimental Results and Model Predictions, *Energy & Fuels*, 18, 1021-1031 (2004)

Biagini E., Cioni M. and Tognotti L., Development and characterization of a lab-scale entrained flow reactor for testing biomass fuels, *Fuel*, 84, 1524-1534 (2005)

Bliek A., Van Poelje W.M., Van Swaaij W.P.M. and Van Beckum F.P.H., Effects of intraparticle heat transfer during devolatilization of a single coal particle, *AIChE Journal*, 31:10, 1666-1681 (1985)

Brewster B.S., Smoot L.D. and Barthelson S.H., Model Comparisons with Drop Tube Combustion Data for Various Devolatilization Submodels, *Energy & Fuels*, 9, 870-879 (1995)

Brown A.L., Dayton D.C., Nimlos M.R. and Daily J.W., Design and Characterization of an Entrained Flow Reactor for the Study of Biomass Pyrolysis Chemistry at High Heating Rates*, Energy & Fuels*, 15, 1276-1285 (2001)

Carpenter A.M. and Skorupska N.M., *Coal combustion — analysis and testing*, IEA Coal Research (1993)

Cetin E., Moghtaderi B., Gupta R. and Wall T.F., Influence of pyrolysis conditions on the structure and gasification reactivity of biomass chars, *Fuel*, 83, 2139-2150 (2004)

Confederation of Finnish Industries, Teollisuuden energiakatsaus 2/2004 (in Finnish), *Internet publication* (2005)

Eaton A.M., Smoot L.D., Hill S.C. and Eatough C.N., Components, formulations, solutions, evaluation, and application of comprehensive combustion models, *Progress in Energy and Combustion Science,* 25, 387–343 (1999)

Finnish Energy Industries, Combined Heat and Power Production, *Ministry of Trade and Industry publication* (2006)

Flagan R.C. and Seinfeld J.H, *Fundamentals of Air Pollution Engineering*, Englewood Cliffs (NJ), Prentice-Hall, Inc. (1988)

Fletcher T., Swelling properties of coal chars during rapid pyrolysis and combustion, *Fuel*, 72:11, 1485-1495 (1993)

Grant D.M., Pugmire R.J., Fletcher T.H. and Kerstein A.R., Chemical model of coal devolatilization using percolation lattice statistics, *Energy & Fuels*, 3,175-186 (1989)

Gronli M., A theoretical and experimental study of the thermal degradation of biomass, *Ph.D. Thesis*, Norwegian University of Science and Technology, Norway (1996)

Gurgel C., Effect of pressure on pyrolysis of wood particles, *Nordic Seminar on Biomass Gasification and Combustion*, Trondheim, Norway (1994)

Hall P.J. and Larsen J.W., Use of Einstein Specific Heat Models to Elucidate Coal Structure and Changes in Coal Structure following Solvent Extraction, *Energy & Fuels*, 7, 42-46 (1993)

Heikkinen J., Characterisation of Supplementary Fuels for Co-combustion with Pulverised Coal, *Ph.D. thesis*, Delft University of Technology, Netherlands (2005)

Hindmarsh C.J., Thomas K.M., Wang W.X., Cai H.Y., Güell A.J., Dugwell D.R. and Kandiyoti R., A comparison of the pyrolysis of coal in wire-mesh and entrained flow reactor, *Fuel,* 74, 1185-1190 (1995)

Hinds W.C, *Aerosol Technology – Properties, Behavior, and Measurement of Airborne Particles*, New York, John Wiley & Sons Inc. (1999)

Holst L.E., Andersson L.A. and Bjerle I., Investigation of peat pyrolysis under inert gas atmosphere, *Fuel*, 70:9, 1017-1022 (1991)

Incropera F.P. and DeWitt D.P., *Fundamentals of Heat and Mass Transfer – 4th edition*, New York, John Wiley & Sons Inc. (1996)

Jamaluddin A.A., Truelove J.S. and Wall T., Devolatilization of Bituminous Coal at Medium to High Heating Rates, *Combustion and Flame*, 63:3, 329 (1986)

Jones J.M., Patterson P.M., Pourkashanian M., Williams A., Arenillas A., Rubiera F. and Pis J.J., Modelling NOx formation in coal particle combustion at high temperature: an investigation of the devolatilization kinetic factors, *Fuel,* 78, 1171-1179 (1999)

Järvinen M., Numerical Modeling of the Drying, Devolatilization and Char Conversion Process of Black Liquor Droplets, *Doctor of Science Thesis,* Helsinki University of Technolgy, Finland (2002)

Kalogirou S.A., Artificial intelligence for the modeling and control of combustion processes: a review, *Progress in Energy and Combustion Science*, 29, 515-566 (2003)

Kinni J., Kouki J., Crombez J-K., Forest Fuel Collection of 1600 GWh per year, *14th European Biomass Conference & Exhibition*, Paris, France (2005)

Kirkinen J., Hillebrand K. and Savolainen I., Turvemaan energiakäytön ilmastovaikutus - maankäyttöskenaario [Climate impact of the use of peatland for energy - land use scenario]. *VTT Tiedotteita - Research Notes 2365*, Espoo, Finland (2007)

Kobayashi H., Rapid Decomposition Mechanism of Pulverized Coal Particles, *S.M Thesis*, M.I.T (1972)

Kokko A. and Nylund M., Biomass and coal co-combustion in utility scale - operating experience of Alholmens Kraft*, 18th International Conference on Fluidized Bed Combustion*, Toronto, Canada (2005)

Koufopanos C.A., Maschio G. and Lucches A., Kinetic Modeling of the Pyrolysis of Biomass and Biomass Components, *Canadian Journal of Chemical Engineering*, 67, 75-84 (1989)

Lehto J., Determination of kinetic parameters for Finnish milled peat using drop tube reactor and optical measurement techniques, *Fuel,* 86:12-13, 1656-1663 (2007)

Lehto J., Development of an experimental laminar flow reactor and a test method for determination of the rate of pyrolysis of high-volatile-content solid fuels, *IFRF Combustion Journal*, Article Number 200702 (2007)

Li S., Xu S., Liu S., Yang C. and Lu Q., Fast pyrolysis of biomass in free-fall reactor for hydrogen-rich gas, *Fuel Processing Technology*, 85, 1201-1211 (2004)

Merrick D., Mathematical models of the thermal decomposition of coal – 2. Specific heats and heats of reaction, *Fuel*, 62:5, 540-546 (1983a)

Merrick D., Mathematical models of the thermal decomposition of coal - 3. Density, porosity and contraction behaviour, *Fuel*, 62:5, 547-552 (1983b)

Merrick D., Mathematical models of the thermal decomposition of coal - 4. Heat transfer and temperature profiles in a coke-oven charge, *Fuel*, 62:5, 553-561 (1983c)

Minkkinen K., Korhonen R., Savolainen I. and Laine J., Carbon balance and radiative forcing of Finnish peatlands 1900-2100 – the impact of forestry drainage, *Global Change Biology*, 8, 785-799 (2002)

Mäkilä M., Turvetutkimusraportti 59/2006 (in Finnish), Geological Survey of Finland, Espoo (2006)

Niksa S., Predicting the Devolatilization Behavior of Any Coal from Its Ultimate Analysis, *Combustion and Flame*, 100, 384-394 (1995)

Nykänen H., Alm J., Silvola J., Tolonen K. and Martikainen P.J., Methane fluxes on boreal peatlands of different fertility and the effect of long-term experimental lowering of the water table on flux rates, *Global Biochemical Cycles,* 12:1, 53-69 (1998)

Oka S. N., *Fluidized Bed Combustion*, Marcel Decker Inc. (2004)

Phuoc T. and Durbetaki P., Pulverized coal conversion in downflow gasifier, *International Journal for Numerical Methods in Engineering*, 24:1,203-218 (1987)

Pyle D.L and Zaror C.A., Heat Transfer and Kinetics in the Low Temperaure Pyrolysis of Solids, *Chemical Engineering Science*, 39:1, 147-158 (1984)

Raffel M., Willert C. and Kompenhans J., *Particle Image Velocimetry – A Practical Guide*, Springer-Verlag Berlin Heidelberg (1998)

Raiko R., Factors Affecting Combustion of Milled Peat in Fluidized Bed, *Tampere University of Technology publication*, 41, Finland (1986)

Rostami, A.A., Hajaligol M.R. and Wrenn S.E., A biomass pyrolysis sub-model for CFD applications, *Fuel,* 83, 1519-1525 (2004)

Saastamoinen J.J. and Aho M.J, The Simultaneous Drying and Pyrolysis of Single Wood Particles and Pellets Made of Peat, American Flame Research Committee, *International Symposium on Alternative Fuels and Hazardous Wastes*, Tulsa, USA (1984)

Saastamoinen J.J., Aho M.J. and Linna V.L, Simultaneous pyrolysis and char combustion, *Fuel*, 72:5, 599-609 (1993)

Saastamoinen J.J., Kiinteän polttoaineen palaminen ja kaasutus, in *Poltto ja Palaminen* (Ed. Raiko R. et al., in Finnish), International Flame Research Foundation, Finland (2002)

Saastamoinen J.J., Aho M.J., Moilanen A., Sorensen L.H., Clausen S. and Berg M., Burnout of pulverized biomass particles in large-scale boiler – Single particle model approach, *Biomass and Bioenergy,* submitted (2006)

Saxena S., Devolatilization and Combustion Characteristics of Coal Particles, *Progress in Energy and Combustion Science,* 16:1, 55-95 (1990)

Shuangning X., Zhihe L., Baoming L., Weiming Y. and Xueyuan B., Devolatilization characteristics of biomass at flash heating rate, *Fuel,* 85, 664-670 (2006)

Solomon P.R., Serio M.A. and Suuberg E.M., Coal pyrolysis: Experiments, kinetic rates and mechanisms, *Progress in Energy and Combustion Science*, 18:2, 133-220 (1992)

Solomon P.R., Hamblen D.G., Serio M.A., Yu Z.-Z. and Charpenay S., A characterization method and model for predicting coal conversion behaviour, *Fuel*, 72, 469–488 (1993a)

Solomon P.R., Serio M.A., Carangelo R. and Markham J., Very rapid coal pyrolysis, *Fuel*, 65:2, 182-194 (1993b)

Sonka M., Hlavac V. and Boyle R., *Image Processing, Analysis, and Machine Vision – 2nd edition*, Thomson Engineering (1998)

Sopo R., Peat*, WEC Survey of Energy Resources 2001*, World Energy Council, *Internet publication* (2001)

Ulloa C., Gordon A.L. and García, X., Distribution of activation energy model applied to the rapid pyrolysis of coal blends, *Journal of Analytical and Applied Pyrolysis,* 71, 465-483 (2004)

Wiktorsson L.-P. and Wanzl W., Kinetic parameters for coal pyrolysis at low and high heating rates – a comparison of data from different laboratory equipment, *Fuel*, 79, 701-716 (2000)

Yu Q., Brage C., Chen G. and Sjöström K., Temperature impact of the formation of tar from biomass pyrolysis in free-fall reactor, *Journal of Analytical and Applied Pyrolysis,* 40-41, 481-489 (1997)

Zanzi R., Sjöström K. and Björnbom E., Rapid high-temperature pyrolysis of biomass in a free-fall reactor, *Fuel*, 75, 5, 545-550 (1996)

Zhang Y.P., Mou J. and Fu W.B., Method for estimating final volatile yield of pulverized coal devolatilization, *Fuel,* 69, 3, 401-403 (1990)

Tampereen teknillinen yliopisto
PL 527
33101 Tampere

Tampere University of Technology
P.O. Box 527
FIN-33101 Tampere, Finland